SimuLase

Typical Examples, Version 2.0

September 30, 2014

Contents

Preface

This manual describes the typical use and the capabilities of **SimuLase**^{TM} for two examples, an edge emitting laser and a vertical external cavity surface emitting laser (VECSEL). It is shown how the program settings are best used for efficient calculation and what information can be extracted from the created data.

1   Edge Emitting Laser

In this example a typical structure for an edge emitting laser is designed and analyzed using **SimuLase**^{TM}. The structure is an $InGaAsP/InP$-based device for operation around $1310\,nm$. Please note that this structure is for illustrative purposes and by no means an optimized device. Some of the results of this example have been published in Ref. [1]. This example can be played through using the free demo version of **SimuLase**^{TM}. The structure, GainDatabase and experimental PL can be downloaded from our website at '**www.nlcstr.com/SimuLaseDemo.htm**'.

Also, the DVD containing the full **SimuLase**^{TM} program contains a directory '**demo_ingaasp**' that contains all data required to reproduce the example of an edge-emitting structure. '**demo_ingaasp**' contains the full structure. '**unbroadened_pl**' contains the GainDatabase for the PL-analysis. '**experimental_pl**' contains the experimentally measured PL spectra and '**broadened_gdb**' contains the GainDatabase for the current calculation. Please note that this example can only be run with the AlInGaPAs-version of **SimuLase**^{TM} and **SimuLase_Designer**^{TM}.

The structure from this example can be downloaded at:
www.nlcstr.com/Download_SimuLase_A/demo_ingaasp.sls
The database can be downloaded at:
www.nlcstr.com/Download_SimuLase_A/InGaAsP_DemoGDB.zip
The experimental PL can be downloaded at:
www.nlcstr.com/Download_SimuLase_A/UsersMeasuredPL.zip

1.1   STEP 1: Setting Up the Structure

When setting up the structure start by setting up the 'quantized region'. This is the sequence of layers containing one or more wells that is used for all microscopic calculations like calculating levels and wavefunctions in the 'Design Structure' window or to set up the gain database. There has to be one and only one connected block of layers that comprise the quantized region. Its layers are marked to be part of that region by checking the box 'Quantized'.

Here, the full structure has four $6\,nm$ wide $In_{0.9}Ga_{0.1}As_{0.53}P_{0.47}$-well wells separated by $10\,nm$ wide $In_{0.863}Ga_{0.137}As_{0.3}P_{0.7}$-barriers. As detailed in the full **SimuLase**^{TM} manual, the calculation effort increases dramatically - about cubically - with the number of wells. Thus, we suggest to only consider one well to be the 'quantized region' (layers 1, 2
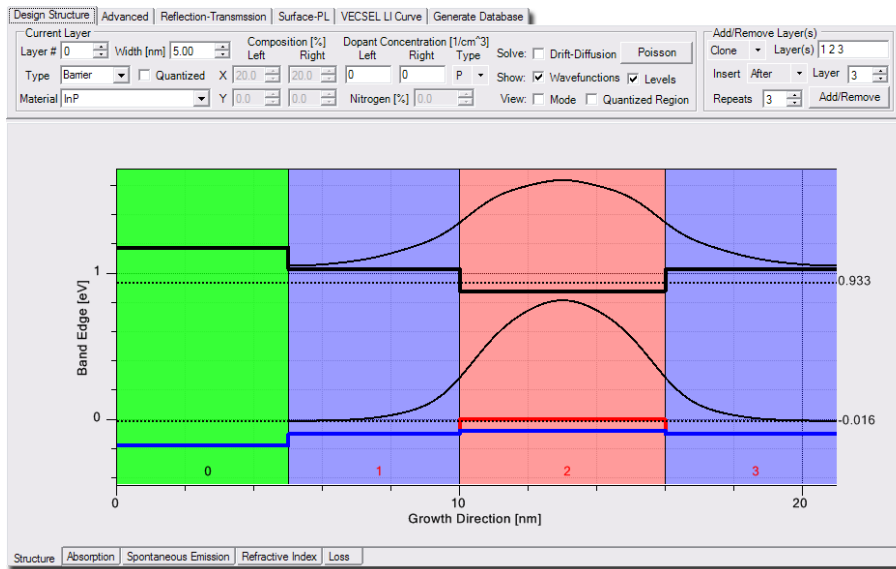
Figure 1: 'Quantized region' of the edge emitting laser (layers 1, 2, 3).

and 3 in Fig.1) and make use of the fact that the microscopic calculations assume periodic boundary conditions. As long as the wells – or at least the energetically lowest subbands that are most crucial for the optical properties – are not significantly electronically coupled and all wells are equally pumped, this approach will yield good results that can simply be rescaled by the total number of wells later. Note that for structures in which structurally different wells share a common chemical potential all wells have to be included in the quantized region in order to obtain correct results for a given pump situation.

The barrier layers 1 and 3 of the 'Quantized Region' should have only half the width of the total barrier width (5nm) since the periodic boundary conditions will lead to an effective width of twice the size. Also, this allows to set up the total active region of the device by simply adding copied of the initial well.

In order to see the influences of strain we temporarily added a layer of the substrate material, InP, as layer '0' that is not marked 'Quantized' before the first barrier.

Layers 1 and 3 are marked as 'Barrier' and layer 2 as 'Well' using the '**Type**' selection. Layer 0 is marked as 'Cladding'. These labels are only relevant if the reflection, transmission or longitudinal (propagating) mode shall be calculated later taking into account data from GainDatabases. Then the absorption/gain for the well/barrier layers is read from the GainDatabases and put in place locally according to these labels.

After setting up the first well and, thus, the 'quantized region', and checking that the electronic levels are at the expected energies, the other wells can be created as copies of the first one. The most efficient way is to use the 'Clone' option and create three clones of layers 1, 2 and 3 and inserting them after layer 3 using the settings for the options in the '**Add/Remove Layer(s)**' sub-panel as shown in Fig.1. By using the 'Clone' option one can later change the layers of all wells consistently by simply applying the change to one of the clones. While the attributes 'well/barrier' will be transferred to the clones, the clones will not be part of the 'quantized region' unless they are manually marked to be part of it.

For this structure the well-region is followed on each side by $35\,nm$ of undoped barrier
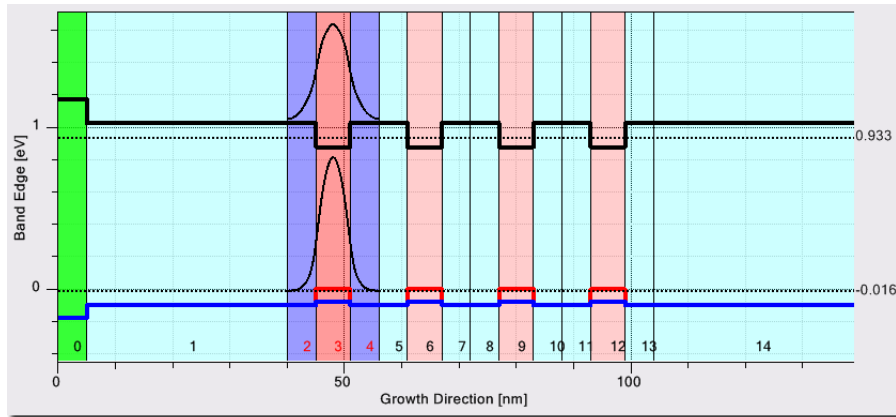
Figure 2: Undoped quantum well and cladding layers of the edge emitting device. The 'quantized region' (layers 1 2 3) is shown in darker blue and pink. The InP-layer '0' has been added temporarily to check for strain.

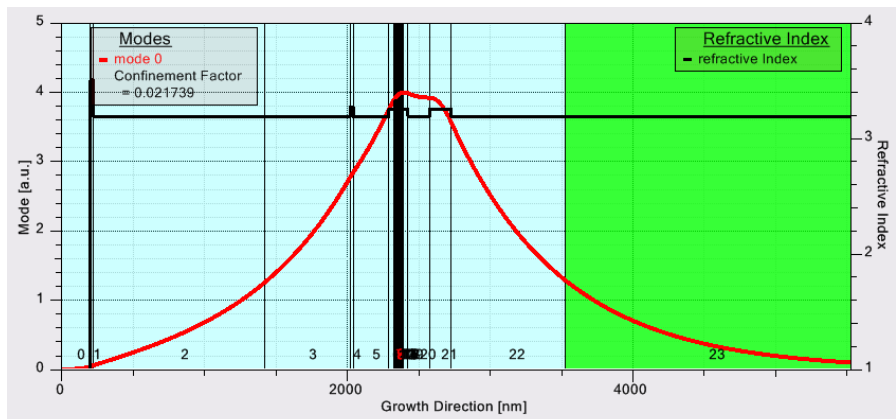material. The resulting structure so far is shown in Fig.2.

Figure 3: Refractive index profile and confined mode of the full edge emitting structure assuming an operating wavelength of $1310\,nm$. Layer '23' is the InP substrate.

The structure is completed by adding n- and p-doped cladding layers of various dopant concentrations and/or material composition. Fig.3 shows the background refractive index profile and the confined mode of the total structure. This view can be accessed by checking the 'View Mode' option. The desired operating wavelength for which the refractive index profile and mode are displayed has to be set on the 'Advanced'-options panel. In order to be able to calculate the optical mode and confinement factor correctly, we also added $200\,nm$ of air (layer '0'), a $20\,nm$ thick metalization layer (layer '1') and $2\,mum$ of undoped InP-substrate.

At this point it is advisable to save the structure using the 'File | Save Structure' dialog. The structural information is saved in xlm-format in a *.sls file. This file can be read also using e.g., Windows Excel. This file can be downloaded from our web site at www.nlcstr.com/Download_SimuLase_A/demo_ingaasp.sls

1.2   STEP 2: Analyzing Experimental PL

With the full structure set up, one can now go ahead and calculate GainDatabase data. If a structure according to this layout has already been grown, the next step should be to perform a PL-analysis. One should compare theoretical to experimentally measured PL-spectra to test the quality of the growth and possible deviations from the design.

The experimentally measured spectra for a PL-analysis should be taken under low but not too low excitation conditions. If the excitation is too weak the PL is dominantly coming from the tail of energetically low defect states and not representing the actual well. Under too strong excitation the PL-lineshape and peak position change strongly with the excitation. Also, the PL can show several and/or poorly defined peaks. Finally, the PL under high excitation is strongly homogeneously broadened due to strong electron-electron scattering. This makes it hard to determine the inhomogeneous broadening that reflects the homogeneity of the growth. All of this makes a PL-analysis very difficult.

Under medium excitation, about 1-20% of threshold, the dominant effect of changes in the pump intensity is mostly a change in the PL-amplitude, the changes in the PL-lineshape are rather small and the PL is usually dominated by a single peak that clearly indicates the (excitonic) bandgap.

Often, the experimental PL is only known for one excitation density. Then, the comparison to the theoretical results can be somewhat inconclusive. While the inhomogeneous broadening and spectral mismatches between design and realization can still be determined with high accuracy, the determination of the intrinsic carrier density is not that conclusive. A more precise analysis can be performed if PL data has been measured for several excitation densities - typically increasing the excitation level by factors of about 1.5 to 3.0.
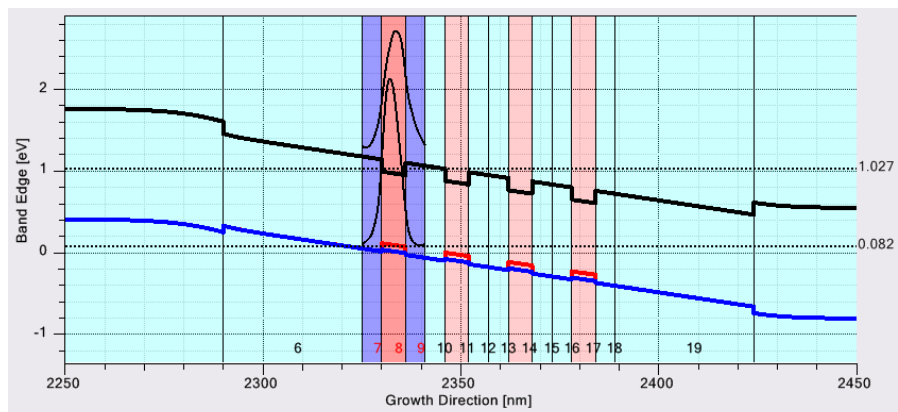
Figure 4: Confinement potential after solving the classical drift diffusion problem to determine the charge potentials due to ionized dopants.

Since the PL is usually measured under optical excitation and without an applied electric pump current and Voltage that compensate the fields from ionized dopants, the theoretical spectra have to take into account these fields. For that, one has to check on the 'Generate Database' panel the option 'Solve Drift-Diffusion'. To take into account also the possible screening of the dopant-related fields due to pump-created carriers one

should also check the option 'Solve Poisson'. Then, the Poisson-Schrödinger problem will be solved for each carrier density.

Next, one has to specify the temperature as it was present in the experiment using the corresponding field on the 'Advance' options panel. If there is only one experimental spectrum (one excitation density), one only needs to set up spectra for two carrier densities, which is the minimum number of carrier densities that are required for a PL-analysis. Typical carrier densities would be 0.1 and $0.2 \times 10^{12}/cm^2$. If one has spectra to more excitation densities one needs to calculate spectra for at least one more carrier density than the number of experimental excitation densities. They should typically span the range between about 0.05 and $1.0 \times 10^{12}/cm^2$.

For a compressively strained structure as in the case here, the PL at low excitation powers will be dominated by TE-polarized light. Select calculating for that polarization using the corresponding option on the 'Generate Database' panel. For other strains one might have to calculate also for TM-polarization.

All other fields of the 'Generate Database' panel can/should be left in their default settings. After hitting the 'Generate Database'-button and selecting a name and directory for the database, the program returns a message about the estimated calculation time and required CPU memory. If these are extremely high (more than maybe 20 minutes per combination of density temperature and polarization) which could be the case for very wide and/or deep wells, one can try to speed up the calculation by resetting the number of subbands that shall be taken into account in the calculation.. Usually the low excitation PL is dominated by emission from the lowest confined subbands. Thus one usually obtains fair results if one only includes maybe 2 or 3 electron subbands and 2 to 5 hole subbands.

Once the database has been successfully created one can load it into the PL analyzer tool '**Tools** | **Analyze Experimental PL**'. For a more detailed description of that tool and the required format for the experimental data see Sec.**??**.
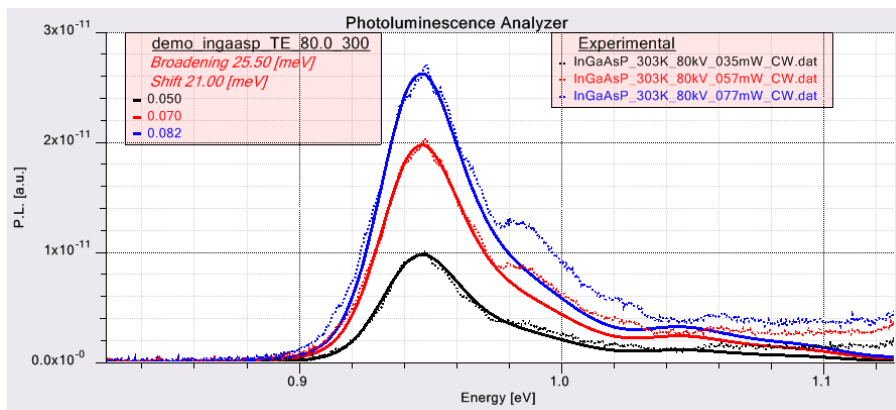
Figure 5: Comparison between measured and calculated PL-spectra using the PL-Analyzer tool.

After loading the experimental data and – since available – subtracting from it a measured background noise spectrum, we find for this structure the result shown in Fig.5. Here, the 'Advanced' options have been used to improve the quality of the agreement. The gain database and experimental spectra for this example can be downloaded from the web at www.nlcstr.com/SimuLaseDemo.htm.

The analysis reveals a spectral mismatch of about $21\,meV$ between the theoretical and experimental spectra. This indicates a small mismatch between the nominal and realized material composition of the well. To a lesser extent this can be explained assuming a mismatch in the well width since typical well width fluctuations influence the transition energies not that strongly. To find out what might explain the mismatch one can vary the 'quantized' well in the 'Design Structure' window and monitor the level energies.

The analysis reveals an inhomogeneous broadening of about $25.5\,meV$ (FWHM). This is the broadening due to local fluctuations in the material compositions and/or the layer widths. The microscopic calculations assume perfect crystals and initially only include the homogeneous broadening due to electron-electron and electron-phonon scattering. The additional broadening can be included by applying a Gaussian broadening to the only homogeneously broadened spectra. This can be done when setting up the initial data by entering one or more broadening values in the corresponding selection box. The calculation will then create in addition to the only homogeneously broadened data copies with the specified inhomogeneous broadening. This has virtually no influence on the calculation time.

A copy of the original database including the determined spectral shift and inhomogeneous broadening can also be created later using 'Tools | Shift and Broaden Database'.

If the determined spectral shift is rather large (about $20\,meV$ or more), one should adjust the parameters of the 'quantized region' and redo the calculation. If the shift is rather small, the only important influence of the deviation between actual and nominal structure is this overall spectral shift. Other results, like lineshapes, amplitudes as function of density and temperature or carrier losses will not be significantly influenced. Thus, one does not have to recalculate the whole database, but can simply apply the shift.

The analysis also shows that the experimental PL has stronger PL at energies above about $0.98\,eV$ than the theory. The theory assumes that all carriers are in thermal equilibrium where they have relaxed to the bottom of the well and are in Fermi distributions. The deviations in the experiment come from the fact that CW-pumping was used under which not all carriers have relaxed to the bottom of the well but some emitted from states in higher subbands. This effect becomes more pronounced with increasing excitation power. It can be avoided by using pulsed excitation.

These energetically higher parts of the spectra should be excluded from the PL-analysis using the option 'Trim Right', from the 'Advanced' option panel.

In a case as here, where the experimental spectra are rather noisy, the analysis can be improved by applying a small broadening to the experimental data using the option 'Apply Smoothing' on the 'Advanced' options panel.

Finally, the analysis also reveals the intrinsic carrier densities that the pump excitation has created. This association between carrier densities and pump excitation can only be performed with a high level of accuracy if experimental data to more than one excitation power is available.

1.3   STEP 3: Setting up a GainDatabase

In general, the database for PL-analysis only needs to be set up for a few densities and one temperature. On the other hand, the GainDatabase for studying the operating characteristics of a device needs to include a larger parameter set.

The carrier densities should cover the full range from low density absorption to the high density gain regime. The density steps also have to be kept small enough to allow for interpolation between them. A typical set of carrier densities for an edge emitting structure would be 0.05, 0.1, 0.2, 0.4, 0.6, 0.9, 1.3, 1.8, 2.4, 3.1, 4.0, 5.0, 7.0, 10.0 and $15.0 \times 10^{12}/cm$ if the 'quantized region' contains only one well. If it contains more wells, these densities should be multiplied by the number of wells. Note, that this is the number of wells for which the microscopic calculations are performed, not the number of wells in the structure.

The temperatures should cover the expected range of operating temperatures. A typical set would cover the range from $275\,K$ to $375\,K$ in steps of $25\,K$.

For highly compressively strained structures (compressive strain larger than about 0.5%) it is usually sufficient to consider only TE-polarized light. For other strains one might have to calculate for TE and TM polarization.

Since the database is for operating conditions where the pump Voltage and current compensate to a high degree dopant related fields, the calculation should be performed for the flat-band case, i.e. with the option 'Solve Drift-Diffusion' , un-checked and the 'External Voltage' left at the default value of zero.

For typical cases where the 'quantized region' has inversion symmetry, it is usually not necessary to include the potential changes due to free carriers (the option 'Solve Poisson'). This option should only be necessary if the well is asymmetric or if electrons and/or holes are not well confined due to very shallow electron and/or hole confinement potentials.

If the inhomogeneous broadening is known from a PL-analysis one should add this value to the list of broadenings. If it is not known one should add one typical broadening. The number of broadenings has no influence on the calculation time only on the memory size of the resulting database. Copies of the database for other broadenings and including overall spectral shifts can be created later using the 'Tools | Shift and Broaden Database'-tool.

All other options should usually be left in their default setting. However, for very wide wells or other situations where the default setting can lead to a situation that would require extraordinary amounts of calculation time, one can use the other settings to reduce the calculation effort - usually at the cost of reduced accuracy. The calculation requirements depend most crucially on the number of required subbands. These numbers are displayed in the message window that appears after hitting the 'Generate Database' button. One can check in the 'Design Structure' window whether all these subbands are really relevant or if some could be left off the calculation since they are energetically too far from the bandedge.

If one decides to set the number of subbands for the absorption/gain or the Auger calculation by hand, one should run a test first for the most extreme case - highest temperature and highest density - how the results change with a change in the number of subbands.

1.4   STEP 4: Determining Operating Characteristics

After having set up the database one can investigate the resulting gain/absorption,
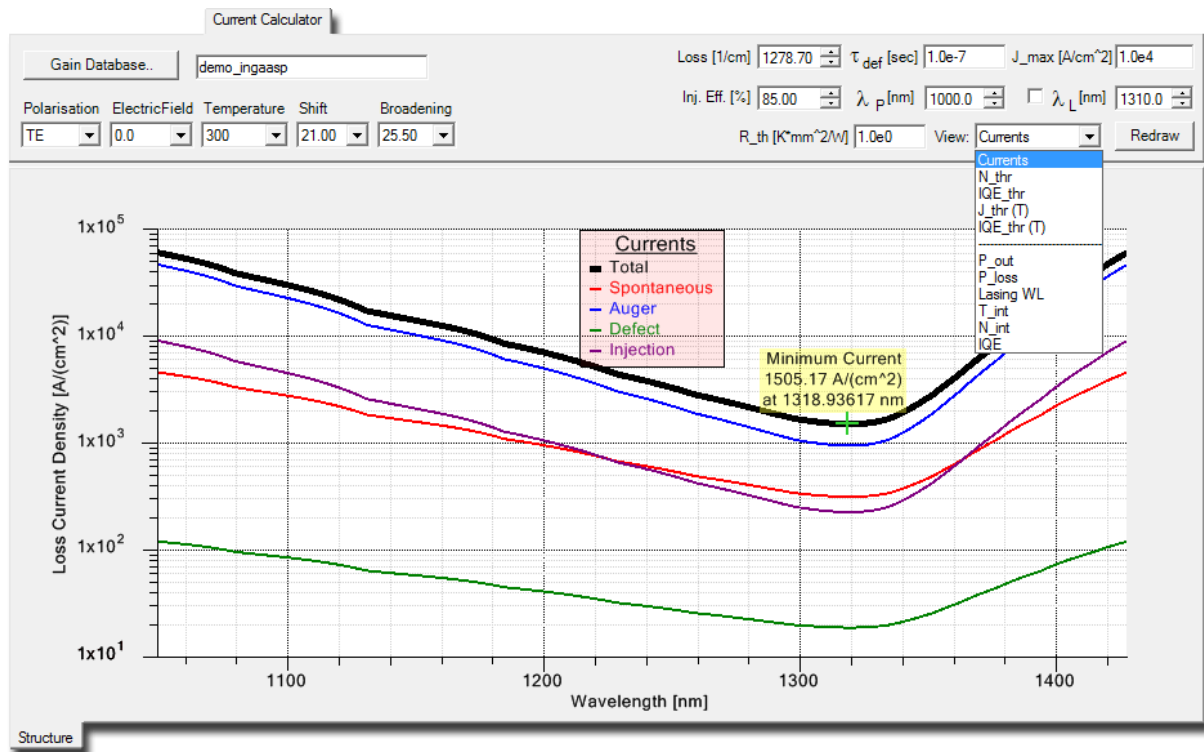
Figure 6: Determining the threshold current and lasing wavelength using the 'Current Calculator' tool.

refractive index and PL spectra using the corresponding display panels. Besides this, **SimuLase**^{TM} offers tools that allow to easily determine some of the most crucial device characteristics like the threshold current and lasing wavelength.

1.4.1   Threshold Characteristics

The threshold characteristics can be determined using the 'Current Calculator'–tool which can be accessed by clicking on the icon ✏ in the top panel or by selecting 'Tools | **Edge Emitter Mode**'.

After the database has been set up one should first apply the spectral shift and inhomogeneous broadening as determined by the PL–analysis using the 'Shift and Broaden Database'–tool. Then one can load this database into the 'Current Calculator' and select the parameters (temperature, polarization,...) for which one wants to know the threshold current.

For this tool to work correctly, the structure has to be present in the 'Design Structure' window. The program determines from the structure the number of wells by counting how many **exact** copies of the quantized region are present in the structure. Since the database has been set up for just one well, the data contained in it will be scaled according to the number of wells as found. The best way to ensure that the intended number of wells is found, the additional wells should be created using the 'copy' or 'clone' option. Otherwise, small modifications of the well or barrier widths may not be transfered correctly to the other wells and they will not be identified as additional 'wells'.

Next, one has to set the material absorption loss in the field 'Loss'. This is the optical loss due to out-coupling and internal losses due to effects like scattering, absorption in un-pumped regions or intraband absorption. The out-coupling loss, α_{out}, can be calculated from the facet reflectivities, $R_{1,2}$, and the device length, L, using:

$$\alpha_{out} = \frac{1}{2L}\,ln\left(\frac{1}{R_1 R_2}\right).$$
(1)

The internal loss, α_{int}, cannot be calculated. It can be measured through cut-back experiments using devices of different lengths. For a real device using the layout and wells as described here the total modal losses have been determined to be $27.8/cm$ with $\alpha_{out} = 17.2/cm$ and $\alpha_{int} = 10.6/cm$.

To convert the modal losses to the material loss units as used in the GainDatabase one has to divide them by the optical confinement factor that can be calculated using the 'View Mode' option within the 'Design Structure' panel (see. Fig.3). Here the confinement factor is 0.02174, resulting in a material loss of $1278.7/cm$.

One also has to specify the injection efficiency in the field '**Inj. Eff.**'. This is the fraction of pump injected carriers that is actually captured into the wells. It can be measured using cut-back experiments. Since this number is not known for the structure here, we use it as an adjustable parameter.

The 'Current Calculator' looks up for each wavelength the gain spectra to find the carrier density that provides enough gain to overcome the material loss. For this density, N, the carrier loss current densities due to defect, radiative and - if available - Auger carrier recombinations, $J_{def/rad/aug}$ are calculated from the corresponding recombination times $t_{def/rad/aug}$ using

$$J_{def/rad/aug} = \frac{e\,N\,n_w}{t_{def/rad/aug}},$$
(2)

where n_w is the number of wells.

These loss currents are plotted together with the injection loss and the total loss for each wavelength.

In an edge emitter without wavelength selectivity, the device would lase at the minimum of the loss current since this is the wavelength where the smallest carrier density/pump current produces enough gain to overcome the optical losses. For the case that the device has wavelength selective gratings or other means to fix the lasing wavelength this wavelength can be specified by checking the box and setting the value in the field λ_L. For both cases, the threshold current and wavelength are marked with a label in the plot.

For a ridge waveguide device based on this structure the threshold current densities were measured to be about $1.23\,kA/cm^2$ at $283\,K$ and $1.45\,kA/cm^2$ at $293\,K$. Interpolating between the minimum threshold values for $275\,K$ and $300\,K$, the analysis would pre-dict threshold current densities of $1.22\,kA/cm^2$ and $1.44\,kA/cm^2$ for these temperatures, respectively, for an injection efficiency of 80%.

Typically, small difference between the theoretical and experimental values should be expected due to some spreading of the pump current in the device. Here we assumed
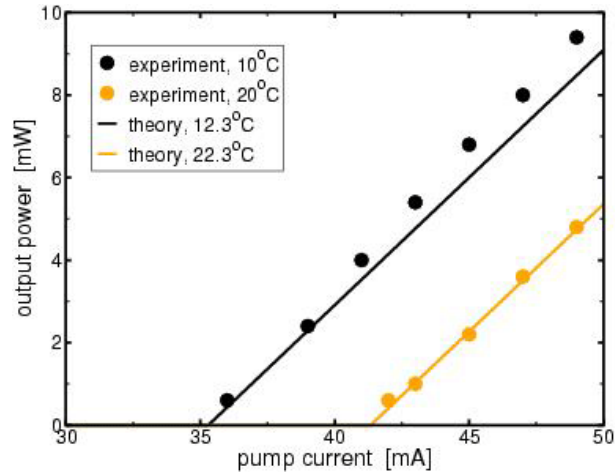
Figure 7: Comparison between experimental and theoretical L–I characteristics (from Ref. [1]).

the pumped quantum well area to be identical to the area of the top contact. Also, some internal heating should occur already at threshold. This could be accounted for by adjusting the injection efficiency. Similar agreement as found here could be achieved assuming an internal efficiency 0f 85% and a small additional heating of about 4K.

Please note that the results here differ somewhat from those in Ref. [1]. This is mostly due to the fact that in Ref. [1]) only spontaneous emission losses into TE–polarized light were included. Here we include losses into TE and TM modes assuming:

$$J_{rad} = \frac{2}{3}J_{TE,rad} + \frac{1}{3}J_{TM,rad}. \tag{3}$$

This leads in this case to a somewhat lower total radiative loss which is compensated for by assuming an injection efficiency that is 80% instead of 100% in Ref. [1].

The tool will always average the TE and TM losses using this formula if spontaneous emission losses for both polarizations are included in the database.

For devices with wavelength selective gratings the loss currents can be determined the same way. Only in this case the loss currents have to be looked up in the 'Current Calculator' at the wavelength determined through the grating and not at the wavelength of minimal losses.

The good agreement between theory and experiment is quite remarkable considering the very limited amount of adjustable parameters. The deviations from the nominal design (spectral detuning and inhomogeneous broadening) were obtained using simple, non–destructive low intensity surface–PL measurements. The only other parameters that needs to be known from the experiment is the internal loss and injection efficiency which can be obtained through cut–back experiments. These losses are usually rather insensitive to details of the structure or situational parameters, like carrier density or temperature. Thus, once they are known for one representative structure, they often can be transferred to investigations of various structures and physical situations without having to be re–measured. No other adjustments were done to all the parameters that are crucially sensitive to details of the structure and the physical situation, like, the gain, its density and spectral dependence or the radiative and Auger losses.

On the other hand, simpler models usually allow for additional fit-adjustments, like, usually, treating the Auger losses as an adjustable parameter. These adjustable parameters allow to **fit** rather featureless characteristics like the threshold. However, this requires the pre-existence of the experimental data and cannot **predict** any results correctly. It will also lead to wrong estimates for the underlying physics and, therefore, prohibit the model to be used to extrapolate to situations/structures that are not very similar to the one for which the experimental data already exists.

This found agreement also demonstrates the importance of correct material characteristics, like gain or Auger and radiative losses, for high quality device simulation. Without this correct input, simulations might wrongfully assume that deviations from the experiment are caused by processes that aren't really a dominant factor, like reduced carrier capture efficiencies or current spreading.
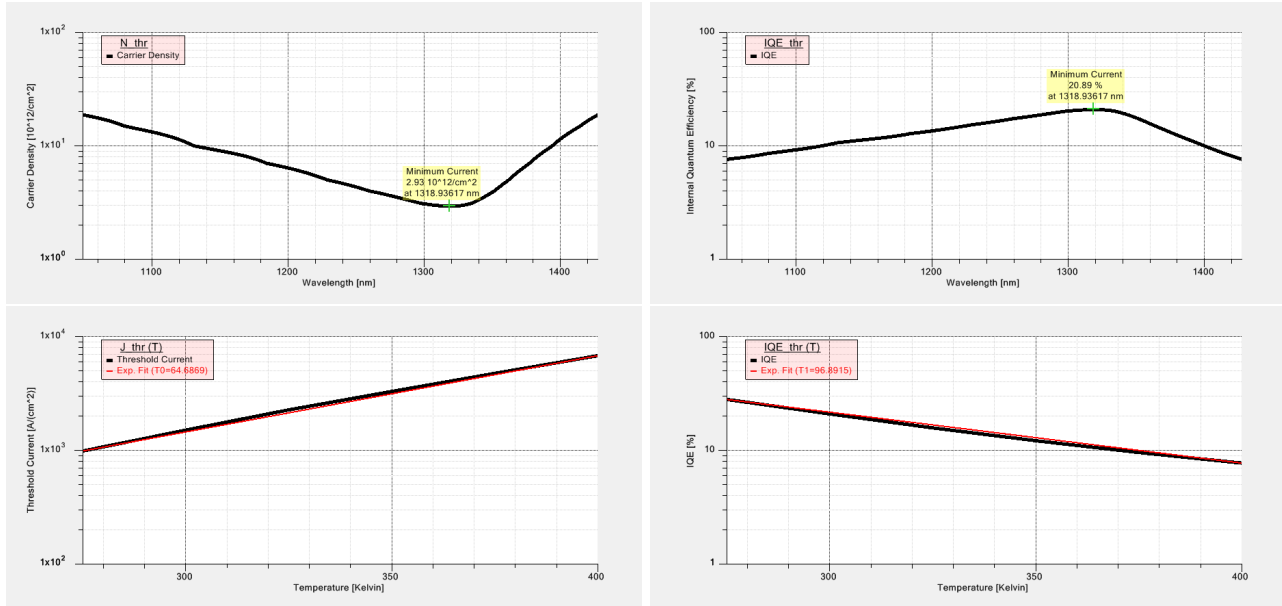

Figure 8: Threshold characteristics calculated using the 'Current Calculator' tool. Top left: intrinsic carrier density. Top right: internal quantum efficiency. Bottom left: threshold current as function of temperature. Bottom right: internal quantum efficiency as function of temperature.

As shown in Fig.8, the tool also allows to display other threshold characteristics: the intrinsic carrier density, internal quantum efficiency, and the temperature dependent threshold current and internal quantum efficiency. The latter two are calculated for all temperatures that are included in the database (shown data is for 85% injection efficiency). Plotted together with them are exponential fits according to:

$$J_{thr}(T) \propto exp(T/T_0)$$
$$IQE_{thr}(T) \propto exp(-T/T_1). \tag{4}$$

The internal quantum efficiency, IQE, at and below threshold is is given by:

$$IQE = \frac{J_{rad}}{J_{total}}. \tag{5}$$

1.4.2   Input-Output Characteristics

For the calculation of the threshold characteristics as described above, internal heating is neglected. With this assumption the results are valid for optical and electrical pumping. For operation above threshold the internal heating is crucially important since, e.g., it will lead to the eventual shut-off of the device.

Since **SimuLase**$^{\text{TM}}$ does not model the electrical pump-injection problem, various heating processes due to it, like Joule heating and Peltier-Thomson heating cannot be taken into account correctly. However, the current calculator tool allows to calculate the input-output characteristics, including the intrinsic heating, for the case of optical pumping. For electrical pumping, this tool can be used as a 'toy' model to study the tendencies of the dependence of the performance on various parameters, like the thermal impedance, number of wells or heat sink temperature.

Like the threshold model, this model requires input for the injection efficiency and optical loss. The model does not account for the temperature dependence of these quantities. Typically, the optical loss increases with increasing pump power and, thus, increasing internal temperature and carrier density. The injection efficiency decreases with pump power. Thus, if possible, these numbers should be adjusted depending on whether one is interested in characteristics near threshold or above threshold.

Besides the input required also for the threshold calculations described above - database, structure, optical loss, defect recombination time and injection efficiency (η_{inj}), the calculations of the input-output characteristics require some additional input to model the internal heating.

Here, the heat sink temperature is given by the temperature set on the 'Advanced' panel. A maximum pump current for which the data shall be calculated has to set in the field '$\mathbf{J}_{max}$'. The thermal impedance of the device has to be specified in the field '$\mathbf{R}_{th}$'. A pump wavelength has to be set in the field 'λ_p'.

In this model the operating characteristics are calculated from the power balance:

$$P_{\text{p}} = P_{\text{out}} + P_{\text{heat}} + P_{\text{rest}}, \tag{6}$$

Where P_{p} is the pump power, P_{out} the output power, P_{heat} power converted to heat and P_{rest} power that is neither converted to heat nor to output power. P_{heat} is determined from the sum of power that goes to pump injected carriers that pass by the wells without being captured, P_{NA}, The excess energy (quantum defect) of carriers being captured into the wells, P_{qd}, Auger losses, P_{aug}, defect losses, P_{def}, and spontaneous emission from the wells that is re-absorbed in the device and converted to heat, $P_{\text{SE-H}}$:

$$P_{\text{heat}} = P_{\text{NA}} + P_{\text{qd}} + P_{\text{aug}} + P_{\text{def}} + P_{\text{SE-H}}$$
$$= \left(1 - \eta_{\text{inj}} \frac{\lambda_{\text{L}}}{\lambda_{\text{p}}}\right) P_{\text{p}} + W \left[\frac{1}{\tau_{\text{def}}} + \frac{1}{\tau_{\text{aug}}} + \frac{1 - \eta_{\text{SE}}}{\tau_{\text{SE}}}\right], \tag{7}$$

$$P_{\text{rest}} = \frac{W \eta_{\text{SE}}}{\tau_{\text{SE}}}. \tag{8}$$

Here, $W = N n_{\text{w}} \hbar \omega_{\text{L}}$, where N is the sheet carrier density, n_{w} the number of wells and $\hbar \omega_{\text{L}}$ the lasing energy. η_{SE} is the fraction of spontaneous emission that is emitted from the wells without being reabsorbed and contributing to heating. η_{inj} is the injection

efficiency. τ_{aug} and τ_{SE} are the microscopically calculated Auger- and radiative lifetimes from the database, respectively. η_{SE} is the fraction of spontaneous emission that is not contributing to heating. The results are usually only very weakly dependent on η_{SE}. We use here a fixed value of $\eta_{\mathsf{SE}} = 0.5$ assuming that 50% of the spontaneous emission escapes through the surface of the device.

The operating characteristics are determined directly from the balance of powers, $P_{\mathsf{pump}} = P_{\mathsf{out}} + P_{\mathsf{heat}} + P_{\mathsf{rest}}$, where P_{heat} is the amount of pump power that is converted to heat and P_{rest} is power lost to spontaneous emission that leaves the device without contributing to heating. For each temperature in the database the intrinsic carrier density at lasing is determined by looking for the density for which the gain is high enough to lead to enough gain to compensate for the optical losses as specified in 'Loss'. If a fixed lasing wavelength has been specified in the field λ_L, the gain has to be high enough at this wavelength. Otherwise, the gain maximum selects the lasing wavelength.

Then, the spontaneous emission, Auger (if present in the database) and defect losses are calculated for this density. It is assumed that all these losses contribute to heating except for a fraction of the spontaneous emission that escapes the device. The results usually do not depend significantly on this fraction. We currently assume that 50% of the spontaneous emission escapes in all cases.

For each pump power, P_{pump}, additional heating losses are given by the amount of carriers that are not captured in the well, $P_{\mathsf{pump}}(1 - \eta_{inj})$, and the quantum defect, P_{qd}, i.e. the difference between pump energy and lasing energy.

The intrinsic temperature increase due to this heating power, ΔT_{heat} is calculated using:

$$\Delta T_{\mathsf{heat}} = P_{\mathsf{heat}} R_{\mathsf{th}}. \tag{9}$$

Finally, the operating point is determined by interpolating between the data for the fixed temperatures of the database in order to look up the temperature, T for which the heating losses lead to a temperature increase satisfying $T = T_{\mathsf{HS}} + \Delta T_{\mathsf{heat}}$. Here T_{HS} is the heat sink temperature. If such a temperature exists for a given pump power the device will lase with non-zero output power.

This model works for optically pumped devices. In electrically pumped devices there is of course no well defined pump wavelength. Carriers will also lose part of their energy to relaxation from the barrier into the wells, but the total energy loss depends on the positions of the Fermi levels, dopant levels and overall band bending due to space charges and applied Voltages - all of which are pump current dependent. Joule heating and Thomson-Peltier heating are not taken into account. Thus, this model is not an exact tool for this situation. It should merely be seen as a help to estimate overall trends in the performance like their variation with optical losses, number of wells or heating as varied with the parameter λ_L.

For the structure investigated here, we find good agreement with the experiment for the threshold current and near-threshold slope efficiencies assuming a thermal impedance of $0.3\, mm^2 K/W$, a pump lasing wavelength of 1000 nm, and the same injection efficiency (80%) and optical loss (1278/cm) as assumed in the threshold calculations. However, with these parameters the simulations do not show any device shut-off within a reasonable pump-current range. The out-put power is terminated only due to the numerics when the intrinsic temperature exceeds the temperature range for which the database was set up (400K).
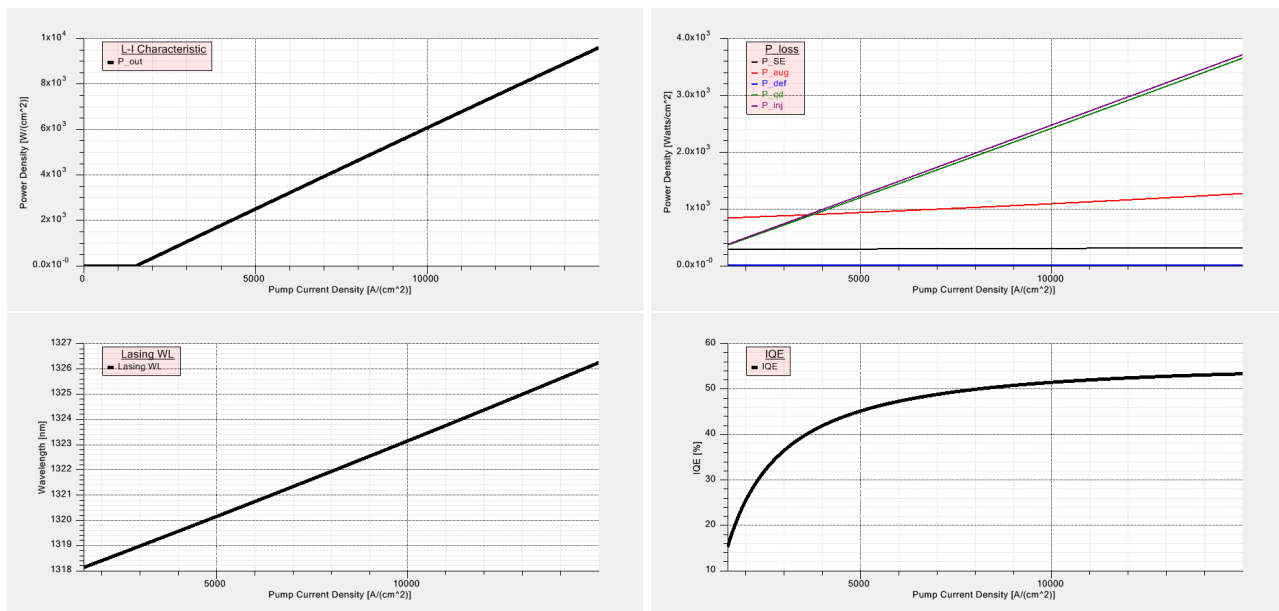
Figure 9: Operating characteristics calculated using the 'Current Calculator' tool assuming an injection efficiency of 80%, a thermal impedance of $0.3\,mm^2K/W$, a heat sink temperature of 293K and an optical loss of 1278/cm. Top left: output power. Top right: various power losses. Bottom left: lasing wavelength. Bottom right: internal quantum efficiency.

This clearly indicates that the optical loss and injection efficiency degrade significantly at elevated pump levels. Shown in Fig.10 is an example where the output power is limited. Here, we assumed an injection efficiency of only 55% and an optical loss of 2100/cm. Obviously, this leads to strong errors in the near-threshold characteristics.

For optically pumped devices the 'injection efficiency' takes on the place of the 'absorption efficiency'. As is explained in the example for an optically pumped VECSEL (Sec.2) this can be calculated rather easily from the calculated absorption spectra. Since in these devices no internal fields should be present, virtually all carriers that are absorbed in the active region will be captured into the wells if proper carrier confinement is provided through SCH or GRINSCH layers. The absorption efficiency varies usually negligibly with the intrinsic temperature or pump power.

Thus, for these cases, the 'injection/absorption efficiency' is no longer a rather free fit parameter. Also, the intrinsic losses usually vary not too much with pump power if the device is not doped – since this eliminates the free carrier absorption which is the main cause for the pump power dependence of the absorption loss. This should typically allow to use this tool very successfully for these situations with an accuracy as is demonstrated for the equivalent case of VECSELs in Sec.2.

1.5   STEP 5: How to Further Use the Data

The microscopically calculated data can also be imported into other simulation software like Crosslight Inc.'s **Lastip**$^{\text{TM}}$ or Rsoft Inc.'s **LaserMOD**$^{\text{TM}}$ for further evaluation of characteristics that go beyond the scope of **SimuLase**$^{\text{TM}}$, like studies of electrical pump
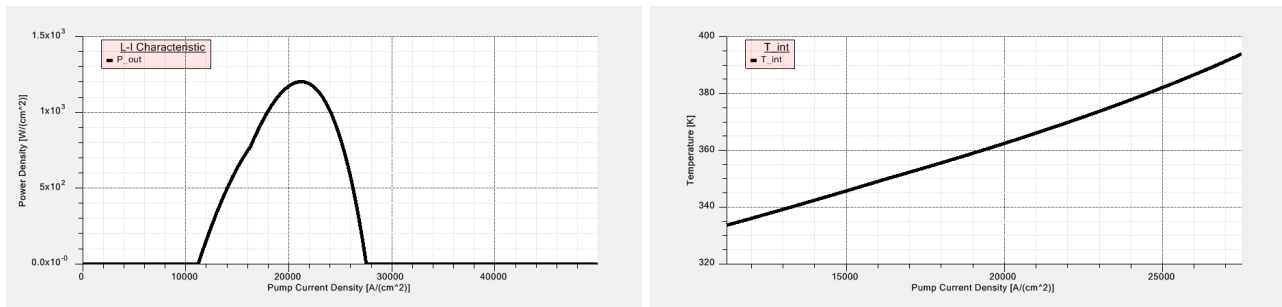
Figure 10: As Fig.9. Here, assuming an injection efficiency of 55% and an optical loss of 2100/cm. Left: output power. Right: intrinsic temperature.

injection, far field broadening or other characteristics that require a model that takes into account in-plane inhomogenities.

For interfacing **SimuLase**$^{\text{TM}}$'s data with Crosslight Inc.'s **Lastip**$^{\text{TM}}$ one has to export the GainDatabase into the format required by Lastip using the option 'File | **Export Database as**'. **SimuLase**$^{\text{TM}}$databases can be directly imported into Rsoft Inc.'s **LaserMOD**$^{\text{TM}}$.

2   Vertical External Cavity Surface Emitting Laser (VECSEL)

VECSELs pose a very hard test to the quality of a modeling tool. These devices are usually driven very hard which leads to internal heating to up to over $400\,K$ at maximum output powers. The wavelength selectivity is provided by a DBR mirror and the resonant periodic gain region (RPG). With heating, the gain shifts spectrally due to the temperature dependence of the quantum well bandgaps. It also changes its lineshapes and amplitudes for a given carrier density due to the changes in the carrier distributions and the changes in the electron-electron and electron-phonon scattering. At the same time the resonance frequency of the RPG-region changes due to the temperature-induced refractive index changes. Ideally one would like to have the gain maximum to spectrally coincide with the resonance of the RPG region at the conditions of maximum output – i.e., at elevated temperatures and high densities.

In order to be able to successfully model this system, the theory has to be able to predict the lineshape, amplitude and spectral position of the quantum well gain correctly for all temperatures and carrier densities. Since the measuring the PL is the best way to test whether the grown material has the desired wells, the theory also needs to be able to predict the PL and its spectral relation to the gain correctly. Carriers that do not contribute to the lasing but recombine due to Auger recombination or spontaneously with the emitted light being re-absorbed outside the pumped region contribute significantly to the heating of the device. Thus, the theory also needs to be able to predict these loss processes correctly.

Without models that can do all that, trying to develop a VECSEL for a given wavelength is destined to require many time and cost intensive iterations of designing, growing and processing, experimentally measuring, analyzing and re-designing. Even if an operating device is achieved, it will be unclear whether it is an optimized solution.

We at NLCSTR have been using the **SimuLase**$^{\text{TM}}$software ourselves to design VECSELs very successfully. One example is the growth of a VECSEL for $1178\,nm$ within a single design-growth iteration. Based on the design developed using the software the growers at NAsP III/V GmbH, Marburg, Germany, grew one wafer after the usual reactor calibration. Processed samples of this first wafer showed output powers up to $9\,W$. After intra-cavity frequency doubling the device showed powers of up to $5\,W$ of $589\,nm$-yellow light emission (see Ref. [5] and our web-site for more information about this example).

Obviously, a complete VECSEL simulation requires modeling of more than the active region and the light propagation within the semiconductor material. It also involves modeling of the heat dissipation and light propagation in the full device – self-consistently with the carrier- and light-creation and losses. However, models for the heat dissipation and light propagation are rather insensitive to details of the active region and the quality of the results will always be far more crucially dependent on the correct microscopic input then the macroscopic modeling.

Here, we use the example of a (not fully optimized) VECSEL for high power operation at $1040\,nm$ to show how **SimuLase**$^{\text{TM}}$can be used to design and analyze such a device. Some of the results shown here can also be found in Ref. [6].

2.1   STEP 1: Setting Up the Structure

As in the case for the edge emitting structure described in Sec.1, one should start set-
ting up the structure with the 'quantized region', i.e. the layers for which the micro-
scopic calculations of the gain/absorption and carrier losses, etc. are to be performed.
Here, this region consists of a $8\,nm$ wide $In_{0.196}Ga_{0.894}As$-well (layer 4) between $5\,nm$
wide $GaAs$-barriers (layers 3 and 5) and $5\,nm$ wide $GaAs_{0.98}P_{0.02}$-barriers (layer 2 and
6). A full period of the resonant periodic gain (RPG) region consists of this 'well' and
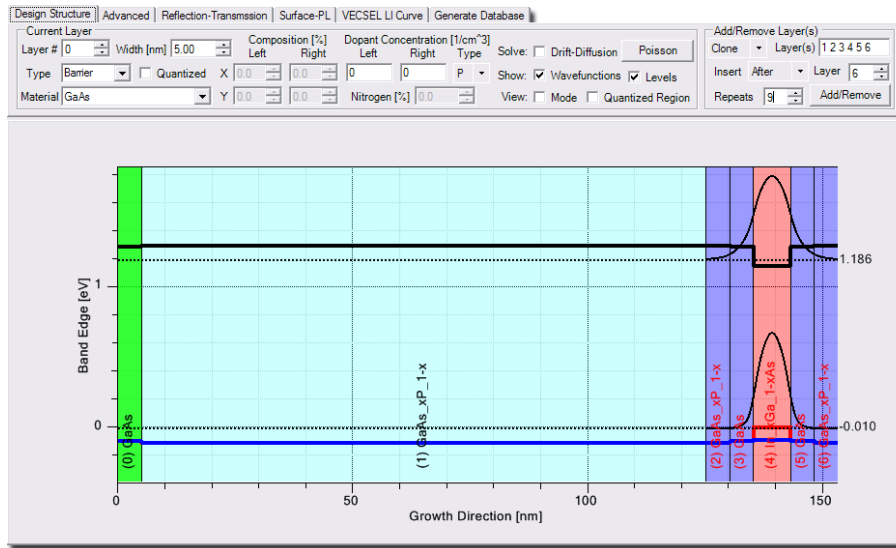$120.4\,nm$ strain compensating $GaAs_{0.98}P_{0.02}$-barrier (layer 1).

Figure 11: One repeat of the RPG-structure of the $1040\,nm$ VECSEL (layers 1-6) including
the 'quantized region' (layers 2-6).

Fig.11 shows the confinement potential of the first period of the RPG. Here, we also
added temporarily a layer of $GaAs$-substrate (layer 0) to see the influences of strain.
Since the device shall be designed to have maximum output power at $1040\,nm$ at an
estimated internal temperature of about $375\,K$, one should set the 'Lattice Temperature'
on the 'Advanced' options panel to $375\,K$. The well has been adjusted such that the
lowest single particle transition energy at $375\,K$ is at about $1040\,nm$.

We only include one well in the 'quantized region' for which the microscopic calculations
will be performed and scale the results according to the actual number of wells after-
wards. Also, we do not use the full RPG-period (layers 1-5) as the 'quantized region'.
Instead, we reduced the thickness of the $GaAsP$ barrier layers by splitting them into
one layer of $5\,nm$ and another layer for the rest. As explained in Sec. 6.4 of the full
manual and for the example of the edge emitter in Sec.1, this is one important way to
reduce the calculation efforts without reducing the accuracy. To assign layers 2-6 to be
the 'quantized region' one has to set the check-mark in field 'Quantized' for these layers.

Layer 4 contains the 'well'-material and has to be assigned the label 'Well' from the
'Type' selection. Layers 1, 2, 3, 5 and 6 have to be assigned the 'Type' 'Barrier'. These la-
bels are only used when the absorption/gain and carrier induced refractive index changes
are assigned to 'well' and 'barrier' layers from the corresponding gain databases in the

calculation of the longitudinal mode and the refraction and transmission spectra using the 'Reflection-Transmission' tool. The 'Type' 'Cladding' is for all layers that are not made of 'barrier' or 'well' material and cannot absorb at relevant wavelengths like $AlAs$-layers in the DBR.
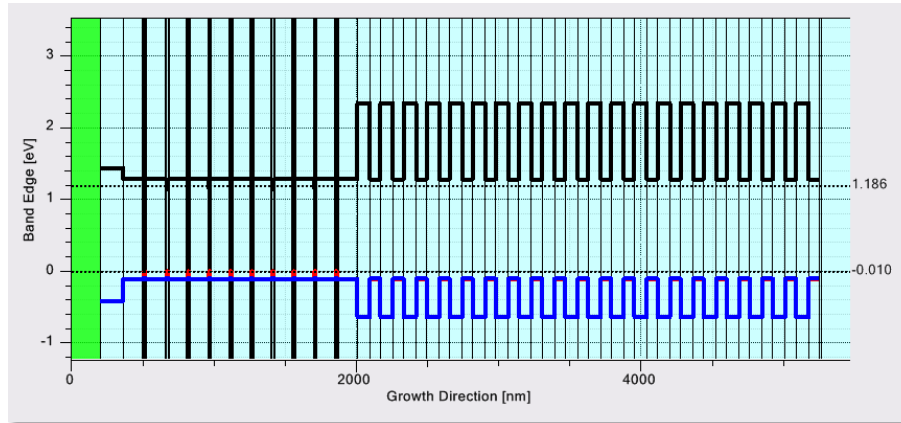

Figure 12: Confinement potential for the full $1040\,nm$-VECSEL structure.

In order to make the full RPG region with 10 wells one should use the 'Clone'-option and 'Insert' 'Layers 1 2 3 4 5 6' 'after' 'Layer 6' making 9 clones by selecting the number of 'Repeats' to be 9 (see the settings in Fig.11).

Using the 'Clone' option rather than 'Copy' has the advantage that one can consistently change the material composition or width of layers in all clones by simply changing them in any one of them. This way, the RPG region can be easily modified in order to get, e.g., the cavity resonance at the desired spectral position.

After cloning the original RPG period, the 'Type's 'Well' and 'Barrier' are copied to the new layers. However, the 'Quantized'-mark is not. Thus, layers 2, 3, 4, 5 and 6 remain the only layers of the 'quantized region'.

After adding some carrier confinement and spacing layers (using the 'Copy' option), the DBR is added. Here again one should start with one period of the DBR and then use the 'Clone'-feature to create the other repeats. Then all periods of the DBR can easily be adjusted simultaneously in order to get, e.g., the stop band in the correct spectral position.

Fig.12 shows the confinement potential of the full structure. Layer 0 is made of air and we added metal layers behind the DBR. Air and metal layers are assigned the 'Type' 'Cladding'. Here, the DBR-repeats are made of $GaAs$ and $AlAs$ layers. The layer 'Type' for the $AlAs$-layers is 'Cladding' and the 'Type' of the $GaAs$-layers is 'Barrier' since the $GaAs$-layers are able to absorb the $808\,nm$ pump light that is used in the experiment.

At this point it is advisable to save the structure using the 'File | Save Structure' dialog. The structural information is saved in xlm-format in a *.sls file. This file can be read also using e.g., Windows Excel.

2.2   STEP 2: Setting up GainDatabases

The next step would be to investigate the longitudinal (propagating) mode and the reflection and transmission of the structure to see whether the nodes and anti-nodes are

at the desired positions – like anti-nodes at the positions of the wells – and whether the DBR-stop-band covers the desired spectral region and the cavity resonance is at the correct position.

While one can do that right away, one should set up GainDatabases for the absorption/gain in the wells and the absorption in the barriers first. Without these, one can only study the un-excited case without pump carriers present. The pump carriers and the induced absorption/gain in the wells and barriers lead to changes in the refractive indices of these layers that shift and modify the cavity resonance and longitudinal mode. For an accurate design of the device at the desired high power operation these changes should be included.

The main GainDatabase is the one for the wells, i.e., the 'quantized region' as it has been defined at the start of setting up the structure (layers 2, 3 4, 5 and 6 in Fig.11). The absorption/gain and carrier induced refractive index changes for this quantized region will be added to the background refractive index in all layers marked as 'Well' through the option 'Type' once the database is loaded into the 'Reflection-Transmission'-tool.
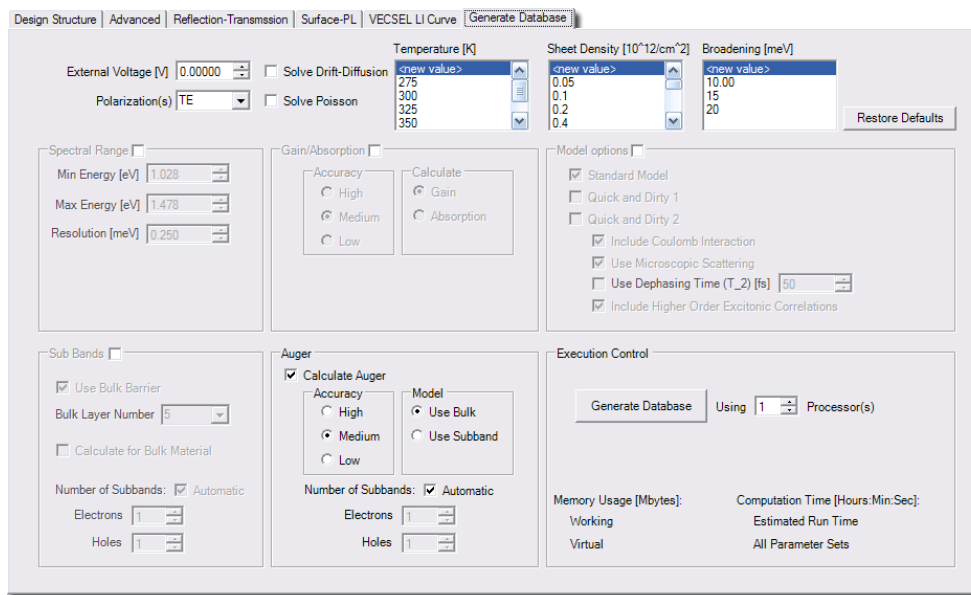

Figure 13: 'Generate Database'-panel with the settings for the calculation of the Gain-Database for the well-layers of the $1040\,nm$-VECSEL structure.

The database can be created with the full structure or just the partial structure as shown in Fig.11 in the 'Design Structure' window since both were set up to contain the same 'quantized region'.

Here, all options in the 'Generate Database' window that are not mentioned below can/should be left in their default configurations. Since Auger losses are important at this wavelength one should check the option 'Calculate Auger'. The only other fields that have to be specified are the values for 'Temperature', 'Sheet Density' and inhomogeneous 'Broadening'. For the purpose of this database we would suggest to calculate for temperatures of 275, 300, 325, 350, 375, and $400\,K$. A typical set of carrier densities would be 0.05, 0.1, 0.2, 0.4, 0.6, 0.9, 1.3, 1.8, 2.4, 3.1, 4.0, 5.0, 7.0, 10.0 and $14.0 \times 10^{12}/cm^2$.

Due to the large compressive strain in this structure the absorption/gain and PL near the bandedge is dominated by contributions from TE-polarization. Thus, and for simplicity of this example, we only set up the well database for this polarization.

The GainDatabase is set up taking into account the homogeneous broadening due to electron-electron and electron-phonon scatterings. The 'Broadening' as specified here is the additional inhomogeneous broadening due to growth fluctuations (see Sec. 7.1.4 of the full manual for details). The number of broadenings as specified here does not influence the calculation time significantly. To cover the typical range of growth conditions one might want to set the database up for broadenings of 10, 15 and $20\,meV$. Copies of the database for additional broadenings can also be created quickly afterwards using 'Tools | Shift and Broaden Database'.

For this set of parameters and this quantized region the calculation time on a typical laptop computer with one CPU takes about 15 hours.

One might not need that many temperatures and densities to just design the device for high power operation. For that purpose two temperatures near the expected high power operating temperature would be sufficient (two in order to allow for interpolations between them) and one would only need densities in the high gain region which is typically above about $3 \times 10^{12}/cm^2$. Additionally one low density is required (typically we use $0.05 \times 10^{12}/cm^2$) in order to be able to determine the change in the carrier induced refractive index. The latter is always calculated by the difference between the values for a given density and the lowest density contained in the database.

Setting up the more comprehensive database is usually worth while. One can then use the database also to analyze low density photo luminescence or to study the device characteristics over the full temperature and excitation range. It also limits possible errors due to interpolations between the datasets.

One often finds afterwards that one would like a database for a slightly different quantized region. This might be due to the fact that the gain maximum at high power operation is found to be not exactly at the desired lasing wavelength. One might also find from experimental measurements of, e.g., the low excitation PL, that the grown device differs slightly from the design. Usually, these changes only amount to small changes in the quantized region like a change in the (Indium-) composition in the quantum well by one or two percent. These deviations usually only amount to a shift of the bandedge transition energy. Other characteristics, like gain amplitudes as function of density or gain lineshapes are virtually un-affected by this. In this cases one does not have to set up a completely new database, but one can simply apply the determined spectral shift to the spectra in the existing database using 'Tools | Shift and Broaden Database'. The 'Reflection-Transmission'-tool includes an option to specify such a shift. Typically, if the required shift exceeds about $15\,meV$ one should consider a re-calculation.

One might also want to set up an additional GainDatabase for the absorption in the barrier layers. While this absorption usually has no significant influence on the characteristics at lasing wavelengths, it can influence the transmission and reflection near the high energy end of the DBR stop-band especially in the case of rather shallow wells. It can also be used to estimate the amount of pump-light that is absorbed in the RPG region.

This database is included in the 'Reflection-Transmission'-calculations through the option 'Use Pre-Computed Database for Barrier Material'. If it is included, the absorption
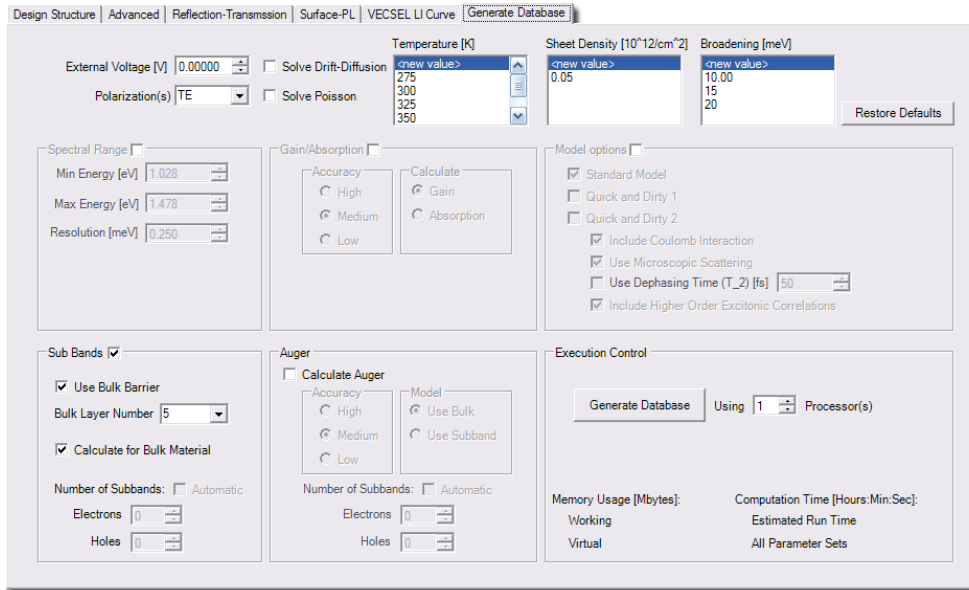
Figure 14: 'Generate Database'-panel with the settings for the calculation of the Gain-Database for the barrier-layers of the $1040\,nm$-VECSEL structure.

is added to the imaginary part of the refractive index for all layers that are marked to be of 'Type' 'Barrier'.

Fig.14 shows the settings one should use for creating this database.

It is assumed that the carrier density in the barriers is negligible due to the large widths of these layers. Thus, this database only needs to be set up for one low density (we use typically $0.05 \times 10^{12}/cm^2$). It should be set up for the same temperatures and inhomogeneous broadenings as the database for the wells.

Since the carrier density of the barriers is assumed to be low, one can neglect Auger losses for this database.

Due to the width of the layers, the barrier material can be described best as bulk material. For this one has to check the options 'Use Bulk Barrier' and 'Calculate for Bulk Material'. In this structure the barrier is made of two materials, $GaAs$ and $GaAs_{0.98}P_{0.02}$. Since the $GaAsP$-layers are much wider than the $GaAsP$-layers we decided here to calculate for bulk-$GaAs_{0.98}P_{0.02}$ by selecting a layer of the quantized region made of this material (layer 2 or 6 of the structure shown in Fig.11) through the field 'Bulk Layer Number'. Since the material properties like the bandgap are very similar for both kinds of materials, we designate this absorption also to the $GaAs$-layers when calculating reflection, transmission or modes. Since the device is pumped optically above the bandgap of both materials, we also use this absorption for both kinds of layers when estimating the pump absorption.

Setting up this GainDatabase only takes about 30 minutes on a single CPU.

For both GainDatabases, the one for the wells and the one for the barriers we use the 'Gain'-model. The pump and lasing wavelengths are longer than about 800nm which is about the shortest wavelength for which we suggest to use the 'Gain'-model. For shorter wavelength the 'Absorption'-model should be used. Also, we are interested in the absorption and gain within the band, not the absorption below the bandgap for which we would suggest to use the 'Absorption'-model.

2.3   STEP 3: Fine-Tuning the Structure

The 'Reflection-Transmission'-tool can be used for some fine-tuning of essential charac-
teristics. For optimum operation one wants to check that the quantum wells are exactly
at the anti-nodes of the longitudinal mode and that the mode has nodes or anti-nodes at
some other interfaces. The stop-band of the DBR should cover the desired wavelength
range and the cavity resonance of the RPG-region should be at the expected lasing wave-
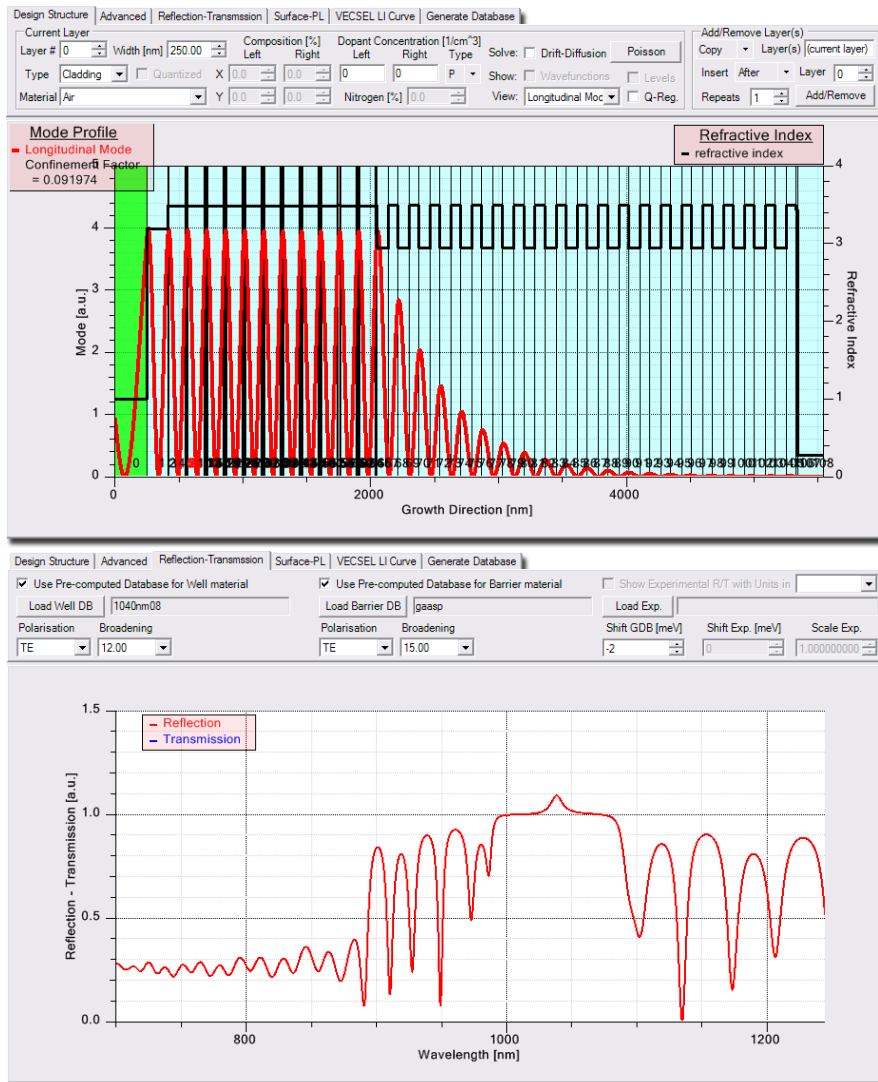length.

Figure 15: Top: Refractive index profile and longitudinal (propagating) mode for the
full $1040\,nm$-VECSEL structure at $375\,K$, $1040\,nm$ and a density of $5 \times 10^{12}/cm^2$. Bottom,
reflection for the same conditions.

Since the device is intended for high power operation these characteristics should be
tested at the expected operating temperature and carrier densities. Thus, one should
first load a GainDatabase that includes the data for the properties of the well material
under the expected conditions. The absorption/gain is then added to the imaginary part

of the refractive index in all layers labeled 'Well' by the option 'Type' on the 'Design Structure' window. The carrier induced refractive index change is added to the real part of the refractive index.
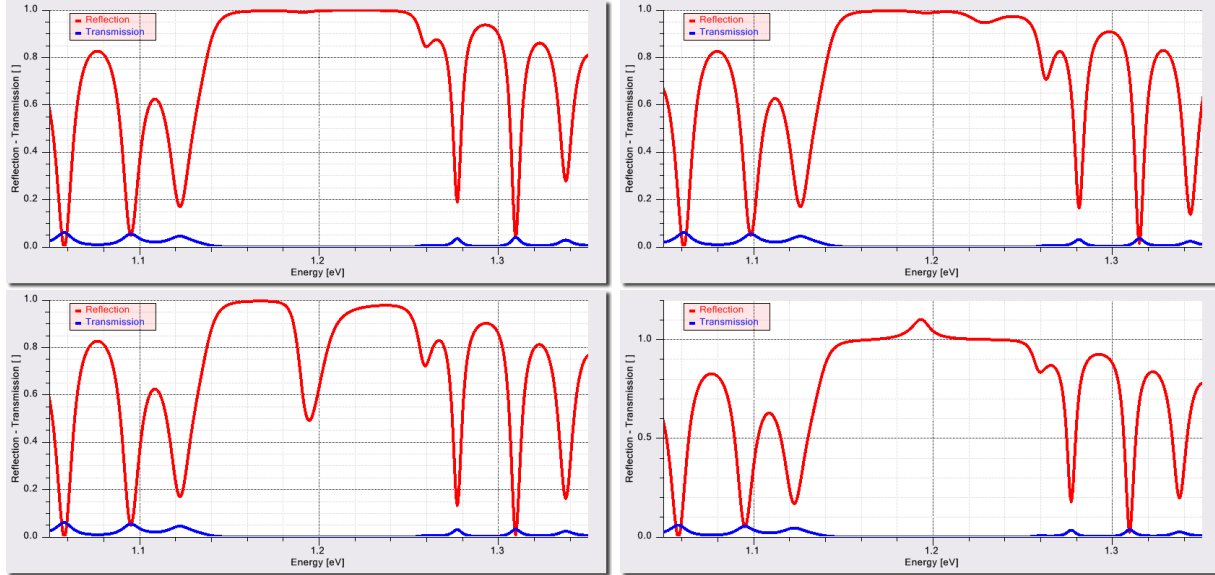

Figure 16: Reflection and transmission spectra of the $1040\,nm$-VECSEL. Top left: $375\,K$, without a database for the well. Top right: $300\,K$, with well-database and zero carrier density. Bottom left: $375\,K$, with well-database and zero density. Bottom right: $375\,K$, with well-database and a density of $5 \times 10^{12}/cm^2$.

Fig.16 shows reflection and transmission spectra for the $1040\,nm$-VECSEL structure. Calculating these spectra without taking into account the absorption/gain in the well layers one finds a flat stop-band with a small cavity resonance dip at the desired wavelength of $1040\,nm$ (about $1.192\,eV$). This shows that the separation of the wells has been chosen correctly. The DBR stop band is at the correct position and wide enough to support operation over the whole expected range of conditions. Also, the reflection is high enough to avoid a noticeable optical loss.

Including the database for the wells leads to a reduction or enhancement of the reflection at wavelengths were the well material has absorption or gain, respectively. In the low density limit the absorption spectra of the well show a well defined excitonic peak at the bandedge. This leads to a dip in the reflection at the excitonic transition energy – here, at about $1.229\,eV$ ($1009\,nm$) at $300\,K$. With increasing temperature the absorption bandedge shifts toward lower energies and eventually coincides with the cavity resonance. This leads to a strong enhancement of the cavity resonance and the absorption dip and cavity resonance are no longer distinguishable.

Once the density is increased (using the corresponding switch on the 'Advanced' panel) and gain occurs at the position of the cavity resonance the reflection at this wavelength becomes larger than one and light at this wavelength will be amplified. The peak of the reflection determines the lasing wavelength.

The enhancement of the reflection is the highest if the gain peak coincides with the cavity resonance. To see whether this is the case one can use the option 'Shift GDB' to shift

the absorption/gain spectra by a certain amount while checking whether the reflection peak increases or decreases.

Here, an out-coupling mirror with 94% reflectivity was used and the internal (surface scattering) loss is estimated to be 1%. Thus, for optimum high power operation one has to find the spectral shift for which the peak in the reflectivity reaches 1.07 at $375\,K$ for the lowest carrier density. We find that a shift of the original database by about $15\,meV$ would be required. The results shown in Fig.16 are for data that has been shifted by that amount. To realize this shift the Indium-composition in the well layers would have to be changed from 19.6% to 18.2%.

2.4   STEP 4: Comparison to the Experiment

While a complete modeling of characteristics of a VECSEL like the input-output power relation requires a model that combines the light propagation/amplification self consistently with the heat- and carrier dynamics (see e.g. Ref. [7]), many important characteristics can be evaluated just using the GainDatabases and the tools within **SimuLase**$^{\textbf{TM}}$.

VECSEL devices with the structural layout as discussed here were grown at the Phillips University, Marburg, Germany, and processed and examined at the University of Arizona and by NLCSTR. The design of these devices did not include the additional shift of about $15\,meV$ that has been found to be optimal in the reflectivity analysis discussed in Sec.2.3. Fig.17 shows the experimentally measured performance characteristics for one of these devices.
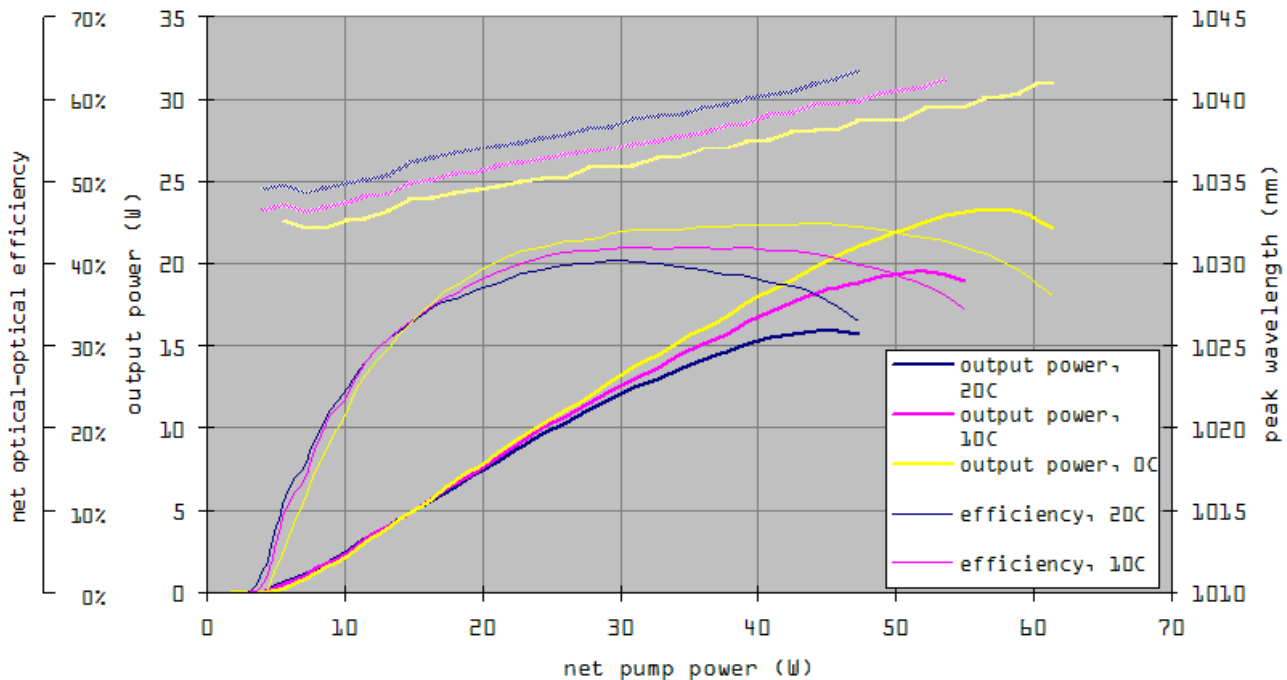

Figure 17: Experimentally measured output power, lasing wavelength and efficiency as function of the net pump power for the $1040\,nm$ VECSEL. Here, an output coupling mirror with 94% reflectivity was used and a pump-spot with a diameter of $550\mu m$.

The first task when evaluating a grown device should be to determine how close the growth has met the design specifications. For a VECSEL the main characteristics that determine the final performance are the spectral position of the cavity resonance, the DBR stop band and the emission wavelength of the quantum wells. The first is given by the distance of the wells, the second by the thickness of the DBR layers and the last by the thickness and composition of the wells.

Two rather easy measurements can be used to determine how close to the design these characteristics are in the grown device. One is to measure reflectivity spectra, the other is to measure surface PL. **SimuLase^{TM}**'s '**Reflection-Transmission**'- and '**Surface-PL**'-tool are designed to allow for an easy analysis of these characteristics.

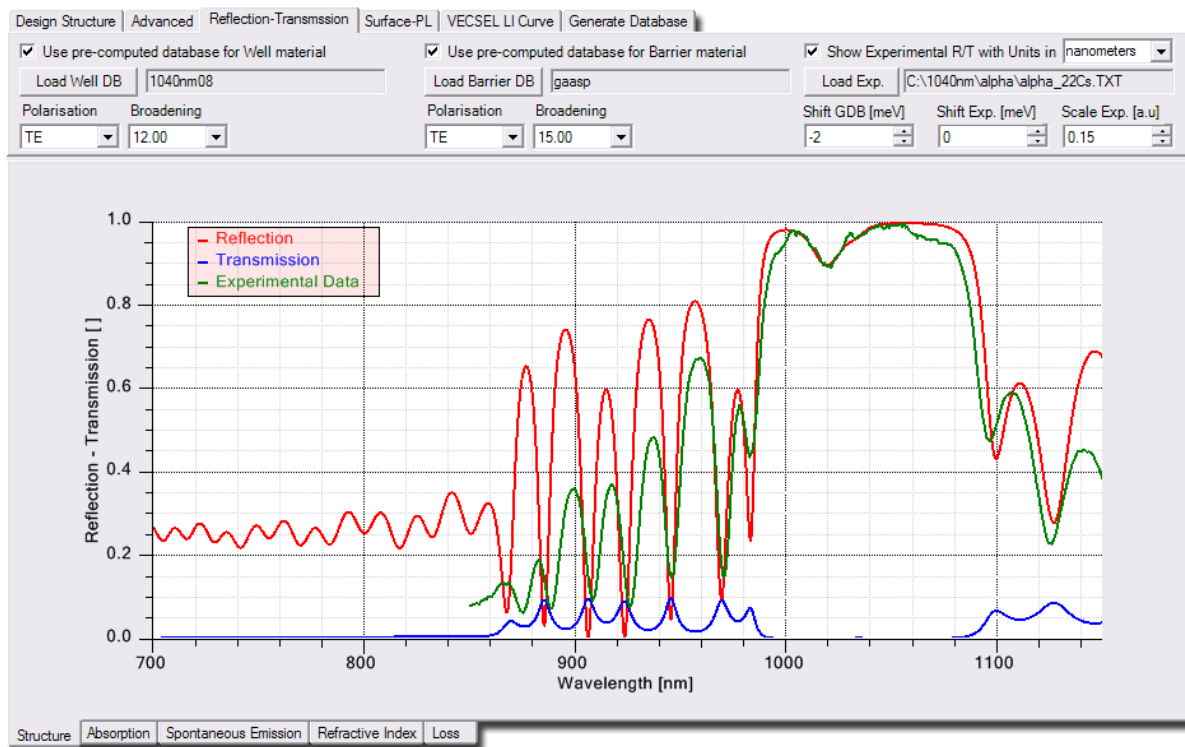### 2.4.1   Reflection Spectra

Figure 18: Comparison between experimentally measured and calculated reflectivity spectra for the $1040\,nm$ VECSEL at 22^oC and very weak excitation using **SimuLase^{TM}**'s '**Reflection-Transmission**'-tool.

Fig.18 shows a comparison between measured and calculated reflection spectra for the 1040nm-VECSEL. The reflection was calculated including a GainDatabase for the quantum well absorption and one for the barrier absorption. Note that the reflection is calculated for the structure that is currently set up in the 'Design Structure' window and for the carrier density and temperature as set in the 'Advanced'-options panel.

The barrier absorption leads to the drop of the reflectivity and transmission for wavelengths shorter than about $870\,nm$. The remaining reflection at shorter wavelengths comes from the surface reflection at the air interface.
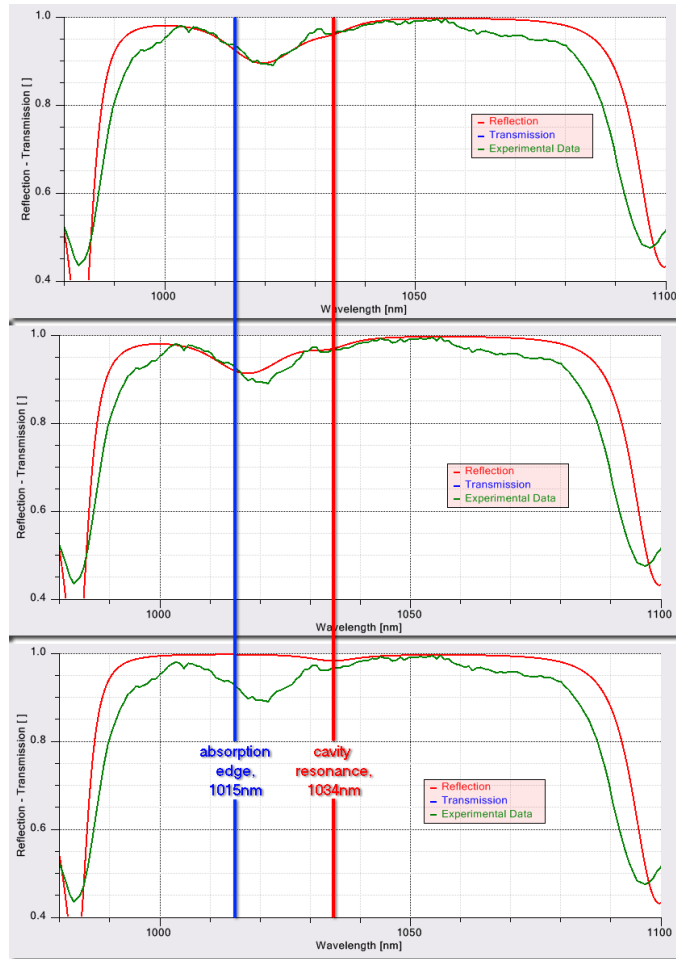
Figure 19: Comparison between measured and calculated reflectivity spectra. Top: After shifting the absorption in the GainDatabases by $-2\,meV$. Middle: For original Gain-Database data. Bottom: Without quantum well absorption. The vertical red line marks the empty cavity wavelength, the blue line marks the excitonic absorption bandedge.

Outside the DBR stop band of high reflection the agreement between theory and experiment is not very good. This is could in part be due to some calibration issues in the experiment which also leads to the deviations at the edges of the stop band. In general this is also caused by the fact that modes at wavelengths outside the stop band are not localized in the active region like the lasing modes shown e.g. in Fig.15. They are delocalized throughout the structure and influenced by all layers, from the top cap layer to the bottom metallization layers. Since these modes are not essential for the lasing operation we do not try to improve the agreement for these wavelengths by fine tuning all layers of the structure.

In order to get the agreement for the reflectivity as shown in Fig.19 we had to shift the DBR stop band by about $5\,nm$ to longer wavelengths by increasing the thickness of the DBR layers by about 0.5%. The cavity resonance appears to be at the designed wavelength, about $1034\,nm$ for this temperature, indicating that the well-separation as in the design. Finally, we had to shift the quantum well absorption spectra of the Gain-Database by $-2\,meV$. This indicates a slightly lower indium-composition in the wells.

Overall, the growth is found in very good agreement with the design.

As can be seen in Fig.19, the reflection analysis is very sensitive to details of the structure. Despite a rather low quality experimental spectrum, the location of cavity resonance and absorption bandedge can be precisely determined and even small deviations, like the $2\,meV$ deviation from the calculated absorption can be easily determined.

Since the dip in the DBR stop band is due to a combination of the well absorption and the (empty) cavity resonance, it is neither at the wavelength of the absorption nor at the wavelength of the cavity resonance. This would make it almost impossible to determine the absorption or cavity resonance without knowing the material absorption precisely.

2.4.2   Surface-PL

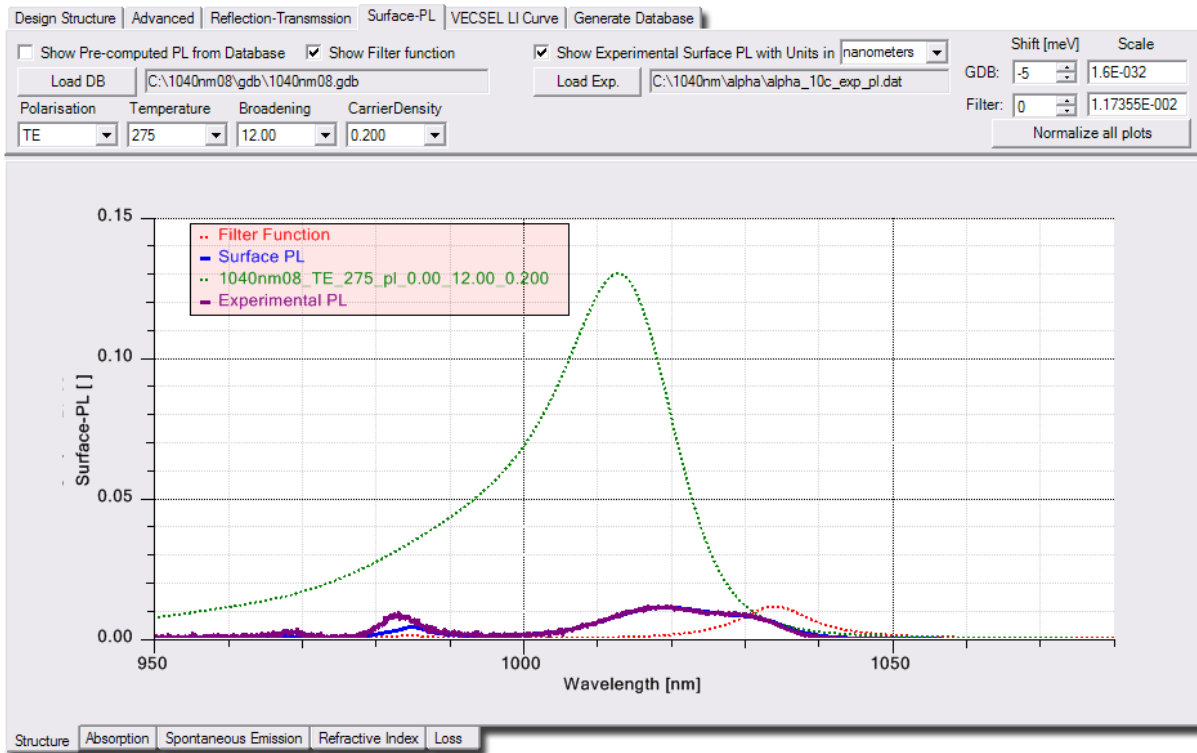Measuring PL-spectra from the surface of the device is one of the most commonly used

Figure 20: Comparison between experimental and calculated surface-PL spectra for the $1040\,nm$ VECSEL at $10^{o}C$ using **SimuLase**$^{\textbf{TM}}$'s '**Surface-PL**'-tool.

tools to analyze semiconductor devices. In structures without strong cavity effects, like typical edge-emitting devices (see Sec.1.2), the surface PL is essentially identical to the pure material PL of the quantum wells that is calculated when setting up a GainDatabase. Here, a direct comparison between the calculated material PL and the PL measured from the surface gives valuable information about the quantum wells.

In structures with strong cavity effects, like V(E)CSELs, the PL is strongly modified on its way from the quantum wells to the surface by reflections at various interfaces and subsequent interferences. This can be seen for the example of the $1040\,nm$-VECSEL in

Fig.20. Here, the cavity effects completely change the lineshape of the PL spectrum. The measured surface-PL has multiple maxima, none of them are at the position of the maximum of the material PL and the lineshape and width of the surface-PL peaks significantly differs from the one of the material PL.

To account for the cavity effects **SimuLase$^{\text{TM}}$**uses the so-called 'Filter-Function Approach' (see Ref. [8]). Here the surface PL is given by the product of the pure material PL of the wells and a filter function that describes the modifications due to cavity effects. Please note that the filter function is calculated for the structure that is currently set up in the 'Design Structure'-window and for the temperature as set on the 'Advanced'-panel. The filter function is independent of the carrier density.
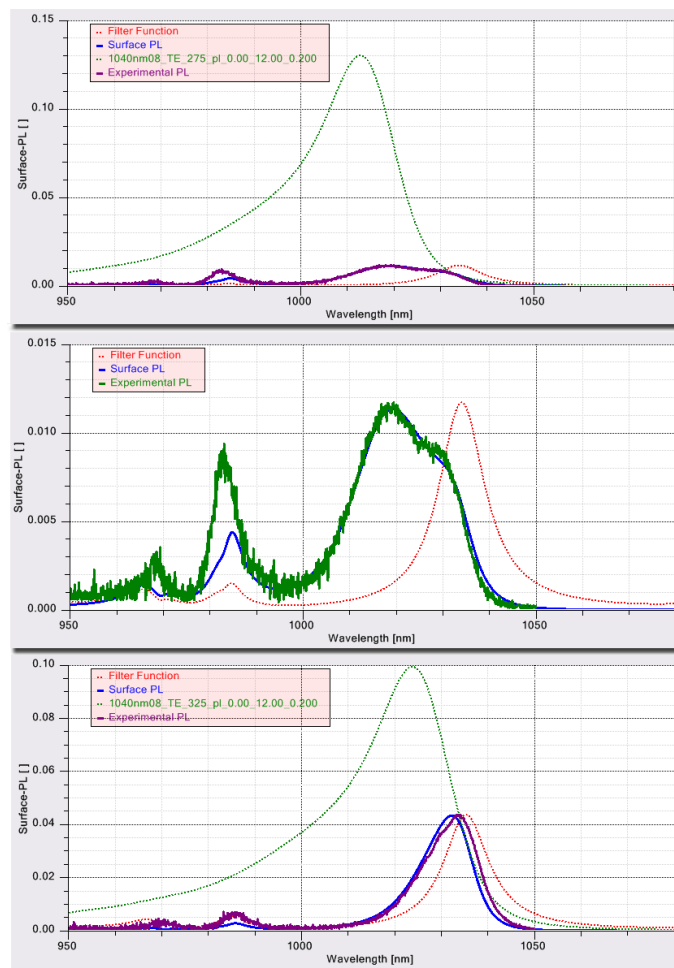

Figure 21: Experimental and calculated surface-PL spectra for the $1040\,nm$ VECSEL. Top: At $10^o C$. Middle, as top, here without showing the material PL. Bottom: At $40^o C$.

For the comparisons shown in Fig.21 the structure was modified according to the deviations between design and actual growth found through the reflectivity analysis. Especially, the same spectral shift has been applied to the pure material PL as the one already determined from the analysis of the reflection spectra. Since the GainDatabase was not set up for the same temperature as in the experiment we used instead the next closest temperature and applied an additional shift to the PL spectra to compensate for

the temperature induced bandgap change. From the comparison we conclude an inhomogeneous broadening of the material PL of about $12\,meV$ (FWHM). This indicates good growth quality with only small local fluctuations in the well width and composition.

The calculated surface-PL agrees very well with the measured one for wavelengths inside the DBR stop band and close to it. As has been seen for the reflectivity, for wavelengths outside this range (shorter than about $980\,nm$) the agreement is less accurate since the modes there are delocalized throughout the structure and we did not attempt to describe them with ultimate accuracy.

For $10^{o}C$, where material PL and cavity resonance are fairly detuned the lineshape of the surface-PL is rather complicated with a double-peak structure inside the stop band and a side peak at the short wavelength side of the DBR stop band. Neither peak is exactly at the position of the maximum of the material PL or the cavity resonance. This shows that an analysis of the surface PL will be quite inconclusive if the correct material PL is not known precisely. Especially, the result depends greatly on details of low and high energy tails of the material PL. Simplified models for calculating the PL will lead to strong errors in these details.

At higher temperatures the material PL and filter function are more resonant. Here the surface-PL is dominated by a single peak at the wavelength of the cavity resonance.

It is noteworthy that the agreement for the surface-PL is achieved for the same deviations between design and actual growth as determined from the reflectivity analysis. As can be seen from the examples shown here, the surface-Pl is very sensitive to exact lineshapes and spectral positions of the cavity resonance, the material PL and the DBR stop band. Thus the '**Surface-PL**'-tool allows for a very accurate characterization of the device.

For the following results we applied this spectral shift and the determined inhomogeneous broadening to the database using 'Tools | Shift and Broaden Database'.

2.4.3   Lasing Wavelength

Fig.22 shows the calculated reflectivity peaks at various temperatures. In the experiment an out-coupling mirror was used that had a reflectivity of 94% (out-coupling loss $L_{out} = 0.06$) and the internal (surface scattering) loss, L_i, was estimated to be about 1%. Thus, for threshold the carrier density has to be high enough to give a maximum reflectivity of about 1.075 to fulfill the threshold condition $L \times R = 1.0$, where L is the total loss, $1 - L_i - L_{out}$, and R is the reflectivity of the chip. The results in Fig.22 are for these threshold carrier densities.

The lasing wavelength at threshold is given by the wavelength of the reflectivity peak. Here it is at $1031.7\,nm$ for $2^{o}C$, $1033.2\,nm$ for $27^{o}C$ and $1034.7\,nm$ at $52^{o}C$. For the temperature that we expect at maximum operating powers, about $100^{o}C$, the lasing wavelength is about $1\,nm$ below the desired wavelength of $1040\,nm$.

In the measurement the lasing wavelength at threshold is found to be about $1033\,nm$ for a heat sink temperature of 0^{C} and $1034.5\,nm$ for $20^{o}C$ (see Fig.17). Comparing these results to the theoretical numbers one finds agreement if one assumes that the internal temperature at threshold is about $25^{o}C$ above the heat sink temperature. Using the GainDatabase in the frame of the comprehensive VECSEL model described in Ref. [7] we find indeed a heating at threshold of just about such an amount.
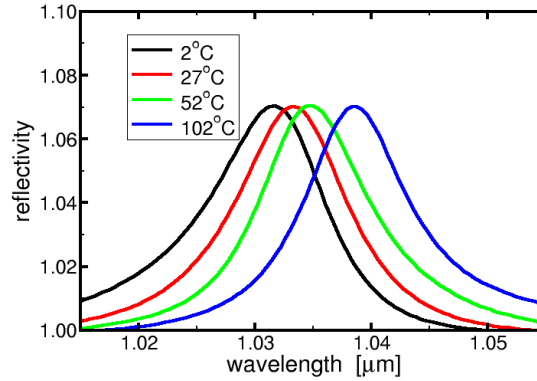
Figure 22: Calculated reflectivity at threshold carrier density for the $1040\,nm$ VECSEL at various temperatures. (Data calculated with and exported from **SimuLase$^{\textbf{TM}}$**.)

In the experiment the lasing wavelength at maximum power is found to be just above $1040\,nm$ (see Fig.17) indicating that the active region of the device reaches temperatures of slightly above 100^oC for these conditions.

2.4.4   Threshold Power

The threshold power, P_{thr}, can be estimated using the simple formula:

$$P_{thr} = \frac{N_{thr}N_w\,A_p\,\hbar\omega_p}{\eta_{abs}\tau_{tot}},\tag{10}$$

where N_{thr} is the sheet carrier density per well at threshold, N_w the number of wells, A_p the pumped area, $\hbar\omega_p$ the energy of the pump light, η_{abs} the pump absorption efficiency and the total carrier lifetime τ_{tot} is connected to the lifetime due to defect-, radiative- and Auger-recombinations via:

$$\frac{1}{\tau_{tot}} = \frac{1}{\tau_{defect}} + \frac{1}{\tau_{rad}} + \frac{1}{\tau_{aug}}.\tag{11}$$

In the experiment the total loss due to out-coupling and surface scattering is about 7%. Thus, the threshold carrier density is determined by using the 'Reflectivity-Transmission'-tool to search for the carrier density that leads to a peak in the reflectivity spectrum of about 1.075. For the resulting threshold power one can look up the carrier lifetimes due to radiative and Auger losses, τ_{rad} and τ_{aug} from the well-database on the 'Loss'-panel. Due to the good growth quality in these devices the defect recombination, $1/\tau_{defect}$, is negligible for densities near or above threshold.

The absorption efficiency is determined from the formula:

$$\eta_{abs} = 1 - exp\left(-\alpha(\hbar\omega_p)\,w_{active}\right),\tag{12}$$

where w_{active} is the width of the active region (wells plus barriers) that can absorb the pump light. For $\alpha(\hbar\omega_p)$ we look up the absorption spectra from the database that we

have set up for the barrier material. Here we find $\eta_{abs} = 0.796$ at 0^oC and it increases to $\eta_{abs} = 0.838$ at 100^oC.

The threshold power can also be obtained using 'Tools | Current Calculator'. Here one has to load the GainDatabase that has been shifted by the $-2\,meV$ determined from the reflection analysis described above and inhomogeneously broadened by the amount of $12\,meV$ determined through the Pl-analysis. The correct value for 'Material Loss' can be looked up in the 'Absorption Window'. Here one has to search for the gain at the wavelength of the reflection peak (lasing wavelength) at threshold density. Since the GainDatabase has been set up for just one well, the value has to be multiplied by the number of wells in the structure. The 'Number of Wells' has to be set to the number of repeats of the 'quantized region' in the structure. Then, the threshold current density is displayed for various wavelengths.

This threshold current density, J_{thr}, is related to the threshold power, P_{thr}, through:

$$P_{thr} = J_{thr} \frac{A_p \hbar \omega_p}{e\, \eta_{abs}}, \tag{13}$$

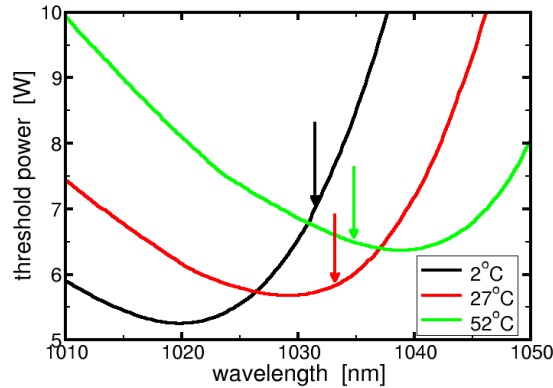For this conversion one can export the current density data using 'File | Export Dataset'.

Figure 23: Threshold power for the $1040\,nm$-VECSEL as function of the lasing wavelength. Arrows indicate the actual lasing wavelengths. Data calculated using 'Tools | Current Calculator' and rescaled according to Eq.(13).

Fig. 23 shows the resulting threshold powers for the $1040\,nm$-VECSEL. Within the scattering of the experiment the theory agrees very well with the experimental threshold values if one assumes the same internal heating above the heat sink temperature by about 25^oC that has been determined in the analysis of the lasing wavelengths. Assuming this heating the threshold power is about $5.9\,W$ for a heat sink temperature of 0^oC and increases to about $6.5\,W$ for a heat sink temperature of 20^oC. Without this heating the threshold power would show the wrong temperature dependence and wrong absolute numbers, decreasing from about $7.3\,W$ at 0^oC to about $6.2\,W$ at 20^oC.

The experimental pump powers at threshold are slightly smaller than in the calculation (see Fig. 17). This is probably due to inhomogeneous pump absorption at these rather

low pump levels. Wells closer to the surface absorb more carriers and reach threshold carrier density earlier than those further away. Effectively this means that the device reaches threshold operating with less than all wells. As can be seen from Eq.(10), such a reduced effective N_w leads to a reduced threshold power. It could also be that at threshold only parts of the pumped area are contributing to lasing. Thus, the effective A_p would be smaller.

At higher pump powers the pump absorption and carrier distribution over the active region become more homogeneous leading to a better agreement between theory and experiment.

In Sec.2.3 we found that the operating characteristics at maximum powers should be better if the design of the wells would be changed such that the absorption/gain is shifted to higher energies by about $10-15\,meV$ (to shorter wavelengths by about $11-17\,nm$). This corresponds to shifting the threshold power curves in Fig.23 by this amount while the lasing wavelength (arrows) stay at the same wavelength or leaving the curves at the same position while shifting the arrows to longer wavelengths. Obviously, this would lead to a strong increase of the threshold power. However, above threshold the increase of the internal temperature with pump power should be decreased which should lead to higher slope efficiency and allow to go to higher pump and output powers before thermal roll over.

2.4.5 Operating Characteristics

Finally, the operating characteristics can be calculated using the '**VECSEL LI-Curve**' tool.
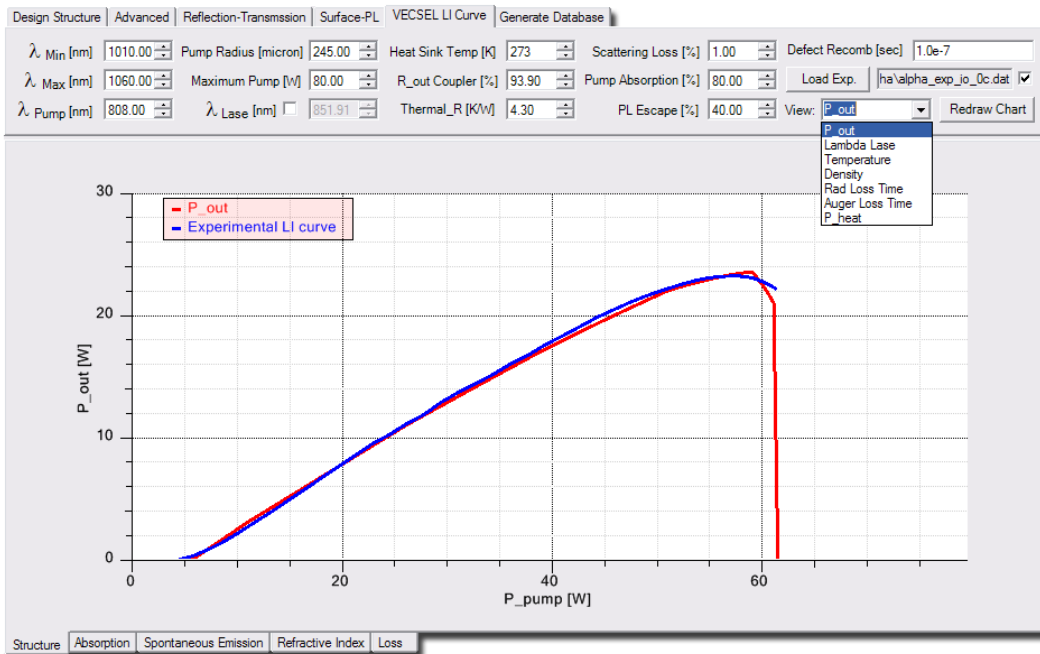

Figure 24: Input–output power characteristic for the 1040nm–VECSEL for a heat sink temperature of 273K. Red: calculated; Blue: imported experimental data.

Here, the characteristics are calculated for the structure currently set up in the '**Design**
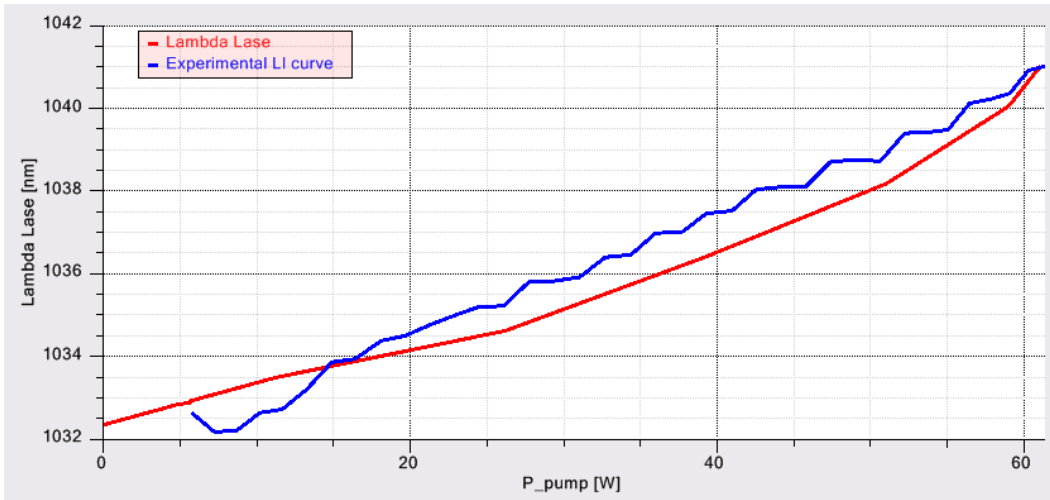
Figure 25: Lasing wavelength as function of the pump power for the 1040nm-VECSEL for a heat sink temperature of 273K. Red: calculated; Blue: imported experimental data.

Structure' and using the GainDatabase for the wells as loaded through the '**Load Well DB**' option on the '**Reflection-Transmission**' panel. The polarization and inhomogeneous broadening, as well as the spectral shift of the well database are also taken over from the corresponding options ('**Polarization**', '**Broadening**' and '**Shift GDB**') on that panel.

The calculations are based on the rather simple one dimensional rate equation model as described in Ref. [7]. I.e., a (circular) top hat profile for the pump spot is assumed and the lasing mode is assumed to have the same shape and size. This simple model is most suitable for situations as here, where the pump spot size is rather large and high power operation is investigated. Then, lateral effects like carrier and heat diffusion from the pump spot into the un-pumped areas are rather negligible. Some deviations between theory and experiment usually occur near threshold with the experimental thresholds usually being lower than the experimental ones. This is caused by lateral and vertical pump inhomogenities. Some wells close to the surface will be pumped stronger than others leading to a situation that resembles one that has fewer wells. Also, unlike in the assumed top hat pump profile, real pump profiles have areas of higher pump intensity. Near threshold this can lead to lasing from a smaller area than the nominal total pump spot. At higher pump powers and correspondingly higher intrinsic temperatures the carriers become more evenly distributed over all wells due to higher carrier scattering rates and mobilities. Also, at powers high above threshold deviations from the average pump intensity become less significant and the pump profile can be better described by a top hat. An interpolation of the experimental characteristic from high powers down shows good agreement with the theoretical results and demonstrates the amount of deviations from the homogeneous situation in the real system.

Apart from the obvious parameters like pump radius, pump wavelength ('λ_{Pump}'), thermal impedance ('Thermal_R'), pump absorption (η_{abs} in Eq.(12)), scattering loss (L_i in the discussion of the lasing wavelength), the out-coupling mirror reflectivity ('R_out Coupler', L_{out}), defect recombination time ('Defect Recomb', τ_{defect} in Eq.(11)) and the heat sink temperature the program also allows to specify the fraction of spontaneous emission that escapes the system versus the one that is re-absorbed in un-pumped areas outside the pump-spot ('PL Escape'). The number set here is the percentage of sponta-
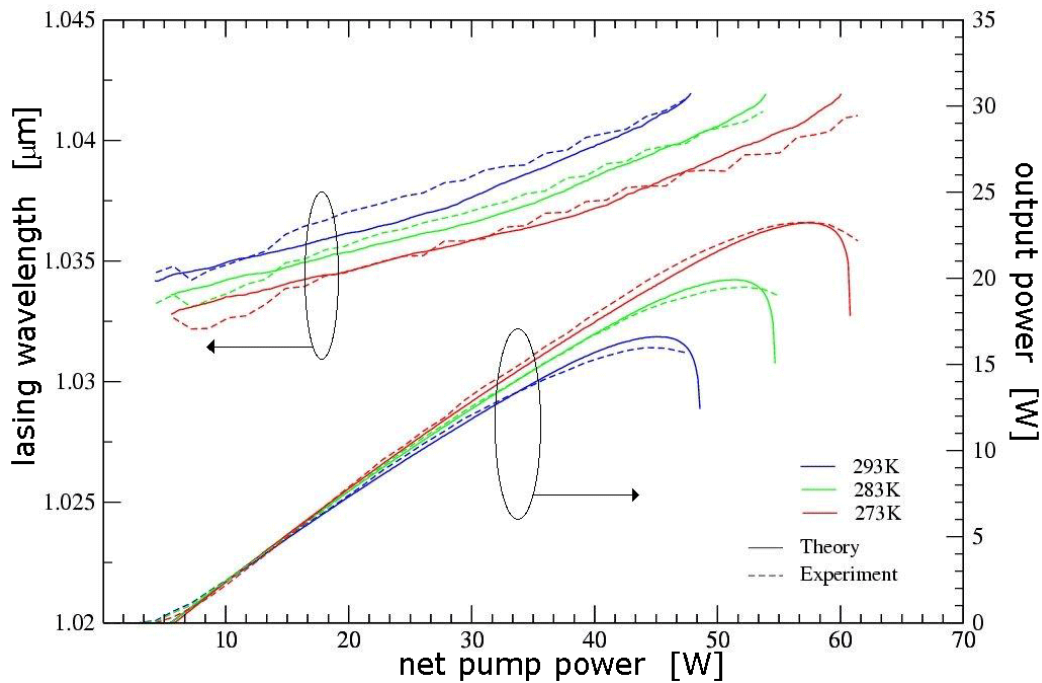
Figure 26: Comparison of theoretical and experimental output powers and wavelength shifts for the $1040\,nm$-VECSEL. Theoretical data calculated with and exported from **SimuLase$^{\text{TM}}$**.

neous emission (PL) that escapes the system. It is assumed that the re-absorbed fraction of the PL contributes to heating. This fraction can be calculated using ray-tracing software. For the example investigated here we found that about 40% of the PL escapes the system. The results are not very critically dependent on this fraction. In our example, the maximum out-put power changes by about 10% when varying the fraction over the whole possible range. The influence on the threshold is even smaller.

The calculation time is only a few seconds. It can be reduced even further by limiting the spectral range that is taken into account in the calculation using the options $\lambda_{\text{Min/Max}}$.

Be default, the spectral range is set according to the spectral range for which the Gain-Database has been set up. Reducing the range typically speeds up the calculation by about a factor of two. Setting the range one has to make sure that it includes all lasing wavelengths for all possible pump powers. Otherwise the correct solution will not be found.

As shown in Fig.26, theory and experiment agree remarkably well for absolute numbers and temperature dependence of all operating characteristics.

For the agreement shown here it was important to include the correct barrier absorption. Only about 80% of the pump light that enters the device is absorbed in the active region and contributes to pumping the wells. The rest enters the DBR layers which are in this case absorbing the pump light. This leads to a reduced efficiency. The pump light that is lost into the DBR acts as a heat source there which further degrades the performance. Overall, the loss of pump light into the barrier reduces the maximum achievable power by about 50%.

The theoretical results are extremely sensitive to many aspects like the correct spectral position of the well-absorption/gain, the correct prediction of the gain amplitude at the

lasing wavelength and the correct prediction of the density that is required to overcome the losses (threshold density) as well as the temperature dependence of all these quantities. Errors in the threshold density will be even further amplified if the models for the radiative and Auger losses are incorrect since these quantities depend even stronger on the carrier density than the gain.

As is shown in more detail in Secs.3 and Sec. 7.2 of the full manual, less sophisticated models than the fully microscopic models implemented in **SimuLase**^{TM} usually result in uncontrolled errors of factors of two or more for quantities like threshold density or radiative and Auger losses and assume wrong dependencies for their density and temperature dependence. In order to compensate for these errors simplified models introduce fit parameters like loss constants for radiative and Auger losses and their dependencies.

SimuLase^{TM} does not require or allow any such adjustable fit parameters which makes its results truly predictive and the theory-experiment agreement as shown here truly remarkable.

3   Summary

Using the tools in **SimuLase**^{TM} allows to design and analyze semiconductor devices effectively and with high accuracy. For the example of a $1040\,nm$-VECSEL we showed how they can be used, e.g., to:

- Design RPG and DBR regions for specific wavelength applications;

- Determine the optimal detuning between cavity resonance and absorption edge;

- Determine growth inhomogenities using PL-analysis;

- Determine deviations from the nominal layer thicknesses and compositions using reflection- and PL-analysis;

- Predict the correct operating characteristics like output-power or the lasing wavelength;

- Show reliably how to optimize devices and

- how close an existing device is to an optimum solution.

Thanks to the predictive quality of the microscopic calculations all these results can be obtained with unprecedented accuracy and without introducing additional fit parameters like radiative or Auger recombination coefficients.

Predicting a quantity like the threshold power and its temperature dependence correct requires all ingrediences of the model to be extremely accurate.

If the gain model fails to predict the threshold density correct the resulting radiative and Auger losses will be off even more. Since these losses increase stronger with the density than the gain, an error of just 20% in the threshold density will result in an error in the threshold power by about 50% or more. As is demonstrated in Sec. 7.2 of the full manual, models for the gain that do not calculate the electron-electron and electron-phonon scattering processes on a microscopic level can easily lead to an error in the threshold density by a factor of two.

Using a simplified model for the spontaneous emission (PL) like the Kubo Martin Schwinger relation usually results in an error for the radiative loss at a given density of the order of a factor of two (see Sec. 7.2 of the full manual). It also leads to errors in the lineshape that make a PL-analysis less conclusive. The latter is especially significant in a surface-PL analysis as shown for the VECSEL in Sec.2.4 where the measured PL is dominated by the high and low energy tails of the material PL.

The density and temperature dependencies that are assumed in simple models for the radiative and Auger losses, like the classical power law $J = AN + BN^2 + CN^3$, are far from reality (see e.g. Sec. 7.2 of the full manual and Refs. [3,4]). The density dependence for the radiative losses in the high carrier density regime in which VECSELs are usually operated tends to be closer to be linear than the quadratic BN^2 law. The density dependence for Auger losses in this regime is also lower than the cubic assumption CN^3 and typically only quadratic.

Since such simplified models cannot predict the operating characteristics correctly one has to introduce additional fit parameters in order be able to reproduce experimental results. Such parameters include the loss constants B and C as well as additional parameters for their temperature dependence. Other models include, e.g., lineshape broadenings for the gain and PL. Even if one is able to reproduce experimental results using such parameters, the underlying physics will be described incorrectly.

Even if a fit to some existing experimental data was successful with a simplified model one usually cannot use the determined parameters to extrapolate to other situations than the ones in the experiment. E.g., since the density and temperature dependencies are wrong in these models one cannot reliably use them to determine high power characteristics from a low power measurement. Since the underlying physical processes are usually very sensitive to structural details like well and barrier compositions or widths, one also cannot use the simplified models to evaluate reliably changes of characteristics due to changes in the structural design.

SimuLase^{TM}is the only commercially available software that includes all the microscopic models that are required for such a highly accurate, quantitatively predictive design and analysis as demonstrated here. For further studies that include e.g. investigations of details like carrier/current- and heat diffusion, **SimuLase**^{TM}allows to easily implement the GainDatabase results into other commercially available software packages using the option File | Export Database as. A ready to use interface with Crosslight Inc.'s software **Lastip**^{TM} already exists.

Current models for those macroscopic properties that determine characteristics like far field broadening, current filamentation or thermal lensing are usually very reliable and accurate. Thus, the overall error of such simulations is usually dominated by the errors that are introduced by using simplified models for the underlying microscopic properties. Therefore, **SimuLase**^{TM}'s GainDatabases offer the ideal - if not required - starting point for such investigations.

References

[1] J. Hader, J.V. Moloney, M. Fallahi, L. Fan, and S.W. Koch, Optics Lett. **31**, 3300 (2006).

[2] L.A. Coldren, and S.W. Corzine, *Diode Lasers and Photonic Integrated Circuits*, (Wiley, NY 1995).

[3] J. Hader, J.V. Moloney, and S.W. Koch, Appl. Phys. Lett. **87**, 201112 (2005).

[4] J. Hader, J.V. Moloney, and S.W. Koch, IEEE J. Quantum Electron. **44**, 185 (2008).

[5] M. Fallahi, L. Fan, Y. Kaneda, C. Hessenius, J. Hader, H. Li, J.V. Moloney, B. Kunert, W. Stolz, S.W. Koch, J. Murray, and R. Bedford, IEEE Photon. Technol. Lett. **20**, 1700 (2008).

[6] J. Hader, G. Hardesty, T.-L. Wang, M.J. Yarborough, Y. Kaneda, J.V. Moloney, B. Kunert, W. Stolz, and S.W. Koch, IEEE J. Quantum Electron., **46**, 810 (2010).

[7] A.R. Zakharian, J. Hader, J.V. Moloney, S.W. Koch, P. Brick, and S. Lutgen, Appl. Phys. Lett. **83**, 1313 (2003).

[8] M. Schafer, W. Hoyer, M. Kira, S.W. Koch, and J.V. Moloney, J. Opt. Soc. Am. B, **25**, 187 (2008).